UCRL 10394

University of California

Ernest O. Lawrence Radiation Laboratory

TWO-WEEK LOAN COPY

This is a Library Circulating Copy which may be borrowed for two weeks. For a personal retention copy, call Tech. Info. Division, Ext. 5545

LONGITUDINAL MIXING IN PACKED GAS-ABSORPTION COLUMNS

Berkeley, California

DISCLAIMER

This document was prepared as an account of work sponsored by the United States Government. While this document is believed to contain correct information, neither the United States Government nor any agency thereof, nor the Regents of the University of California, nor any of their employees, makes any warranty, express or implied, or assumes any legal responsibility for the accuracy, completeness, or usefulness of any information, apparatus, product, or process disclosed, or represents that its use would not infringe privately owned rights. Reference herein to any specific commercial product, process, or service by its trade name, trademark, manufacturer, or otherwise, does not necessarily constitute or imply its endorsement, recommendation, or favoring by the United States Government or any agency thereof, or the Regents of the University of California. The views and opinions of authors expressed herein do not necessarily state or reflect those of the United States Government or any agency thereof or the Regents of the University of California.

Research and Development

UCRL-10394
UC-4 Chemistry
TID-4500 (17th Ed.)

UNIVERSITY OF CALIFORNIA
Lawrence Radiation Laboratory
Berkeley, California

Contract No. W-7405-eng-48

LONGITUDINAL MIXING IN PACKED GAS-ABSORPTION COLUMNS

William E. Dunn, Theodore Vermeulen,
Charles R. Wilke, and Tracy T. Word

July 31, 1962

Printed in USA. Price $1.75. Available from the
Office of Technical Services
U. S. Department of Commerce
Washington 25, D.C.

UCRL-10394
UC-4 Chemistry
TID-4500 (17th Ed.)

UNIVERSITY OF CALIFORNIA
Lawrence Radiation Laboratory
Berkeley, California

Contract No. W-7405-eng-48

January 14, 1963

ERRATA

TO: All recipients of UCRL-10394 UC-4 Chemistry

FROM: Technical Information Division

Subject: LONGITUDINAL MIXING IN PACKED GAS-ABSORPTION COLUMNS by William E. Dunn, Theodore Vermeulen, Charles R. Wilke, and Tracy T. Word July 31, 1962.

OK

Please replace Figure 23, page 49, in your copy of the subject report with the attached.

LONGITUDINAL MIXING IN PACKED GAS-ABSORPTION COLUMNS

Contents

Abstract v

Introduction 1

Theoretical 4

Random-Walk Model 4

Diffusion Model 5

Experimental 11

Apparatus 11

Procedure 27

Packing Characteristics 28

Results and Conclusions 30

Application to Design 46

Acknowledgments 54

Notation 55

Appendix 57

References 64

LONGITUDINAL MIXING IN PACKED GAS-ABSORPTION COLUMNS

William E. Dunn, Theodore Vermeulen,
Charles R. Wilke, and Tracy T. Word

Lawrence Radiation Laboratory and Department of Chemical Engineering
University of California, Berkeley, California

July 31, 1962

ABSTRACT

Longitudinal-mixing experiments were conducted in a 2-ft-diam gas-absorption column by using tracer-injection techniques. The carrier streams were air and water.

Empirical Peclet-number correlations are presented for both phases, with 1-in. Berl saddles, 1-in. Raschig rings, and 2-in. Raschig rings used as packing materials. The extent of mixing was much greater in the liquid phase than the gas phase. Gas-phase Peclet numbers decreased with both liquid and gas flow rates. On the other hand, liquid-phase Peclet numbers were found to increase with liquid flow rates, and no quantitative effect of gas rate was observed.

Methods are outlined that illustrate the application of the data to mass-transfer systems. By means of examples, it is shown that mixing can contribute significantly to absorption-column design requirements. This factor becomes more pronounced in liquid-phase-controlled diffusion.

INTRODUCTION

Packed columns are used frequently in industry for gas-absorption or stripping operations. In designing such columns one generally obtains an estimate of the tower height by multiplying the total number of transfer units by a correlational height of a transfer unit.

The NTU (number of transfer units) concept was first introduced by Colburn.[1, 2] In relating the NTU to stream compositions Colburn makes a material balance that inherently assumes a piston-flow model for both phases. In previous work[5] it is shown that the effect of axial mixing, a deviation from piston flow, may be a significant design factor for liquid-liquid extraction systems in packed columns.

The phenomenon of axial mixing arises from the fact that "packets" of fluid do not all move through a packed bed at a constant and uniform velocity. This may result from (a) velocity gradients as the fluid flows through the packing and or (b) eddy motion of the fluid itself. The former is more characteristic of a laminar-flow regime, whereas the latter is probably more characteristic of turbulent flow.

Axial mixing tends to reduce the concentration driving force for mass transfer from that which would exist for piston flow. This reduction is illustrated in Fig. 1 where the concentration profiles for piston flow are the dotted lines, and the solid lines represent the axial-mixing case.[6] Note that there is a discontinuity at the points where the countercurrent streams enter the extractor when mixing is present. To achieve a given separation, more transfer units are required for the axial-mixing case owing to the reduced driving force. Likewise, for a given column under conditions of axial mixing, HTU's (heights of a transfer unit) reported on the basis of on the Colburn equations, are higher than the true HTU's that would be calculated from the actual mass-transfer coefficients.

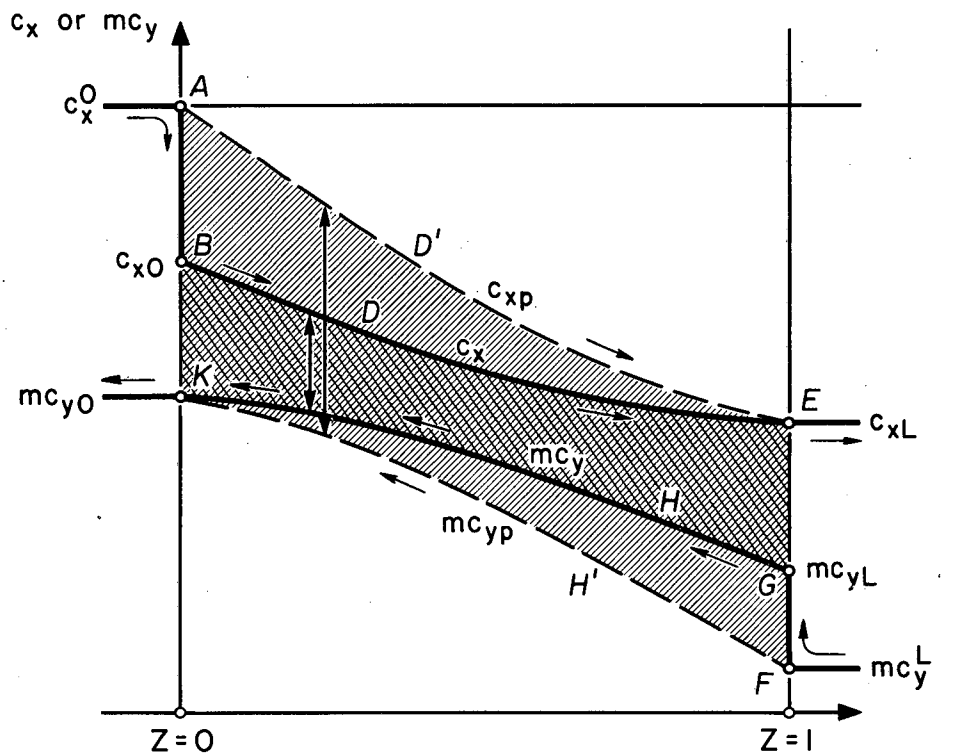

MU-14083

Fig. 1. Concentration profile in a typical extractor (after Miyauchi).

Our object in this study is to determine whether axial mixing is an important factor in gas-absorption column design, and to provide correlations of dispersion coefficients in the form of Péclet numbers for both liquid and gas phases.

Stemerding[11] has reported axial-dispersion coefficient data for the water phase measured in an air-water system flowing through a 400-mm-diam column packed with 13-mm Raschig rings. He found that the dispersion coefficients were in the range of 8 to 15 cm^2/sec, and were relatively insensitive to gas and liquid flow rates.

Otake and Kunugita[9] have reported Péclet numbers for single-phase water flow in a laboratory-sized column. They found the Péclet number to vary approximately as the one-half power of the superficial velocity.

THEORETICAL

The extent of axial mixing may be evaluated quantitatively, independently of any mass transfer, by tracer-injection techniques. A tracer amount of a component is injected into one of the bulk phases in the form of a step, impulse, or sine-wave input. A step input was used as a basis for this study. The buildup of tracer at a fixed distance downstream from the injection point is measured as a concentration-time relation which is called a breakthrough curve. The characteristics of the experimental breakthrough curve may then be compared with the forms predicted by a mathematical mixing model; the value of the mixing parameter in the mathematical model that gives the best fit to the experimental curve is designated as the mixing parameter characteristic of the experimental system. Two such models were found to be pertinent to the case at hand, and their results are briefly described.

Random-Walk Model

The random-walk model is characterized by "packets" of fluid moving through the packing in a series of discrete jumps corresponding to a certain mean free path, l, and with a characteristic velocity, u. If the total bed length is h, and the time that a packet of fluid has been in the bed is t, then the number of mixing lengths (or column Péclet number) is defined as h/l, and the dimensionless-time scale, T, as ut/l. If a step input of tracer with magnitude C_0 has taken place at $N=0$ and $T=0$, it develops that

$$x = \frac{C}{C_0} = \int_0^{T'} \exp(-N-\tau)\, I_0\left(2\sqrt{N\tau}\right) d\tau, \qquad (1)$$

where τ is the dummy variable of integration, and $T' = T(N+1)/N$. The solution to this integral equation is shown graphically in Fig. 2 as a semilog plot of dimensionless concentration vs log dimensionless time for several values of N, the column Péclet number. Here the time scale has been normalized about the stoichiometric time (the time required to replace one column holdup of the phase of interest), at which $T=N$.

To compare these results to experimental curves, it was expedient to compute the midpoint slopes s relative to a time scale of $t_{(x=0.5)}$; i.e.,

$$S = \frac{dx}{dT} \times T_{(x=0.5)} \tag{2}$$

A numerical approximation to the above equation solved for N was found to be[5]

$$N = 4\pi s^2 - 0.80. \tag{3}$$

Now the column Péclet number based on the random-walk model may be evaluated explicitly from an experimental breakthrough curve by evaluating the midpoint slope and substituting in Eq. (3). The packing Péclet number, P, is proportional to the column Péclet number, N, with a proportionality constant d_p/h (or B). Hence, N is equivalent to PB.

Diffusion Model

An analogy between open-pipe flow and flow through a packed bed is assumed in the diffusion-model approach. The general one-dimensional diffusion equation may be expressed

$$\frac{\partial^2 C_i}{\partial Z^2} - N_i \frac{\partial C_i}{\partial Z} = N_i^2 \frac{\partial C_i}{\partial T}, \tag{4}$$

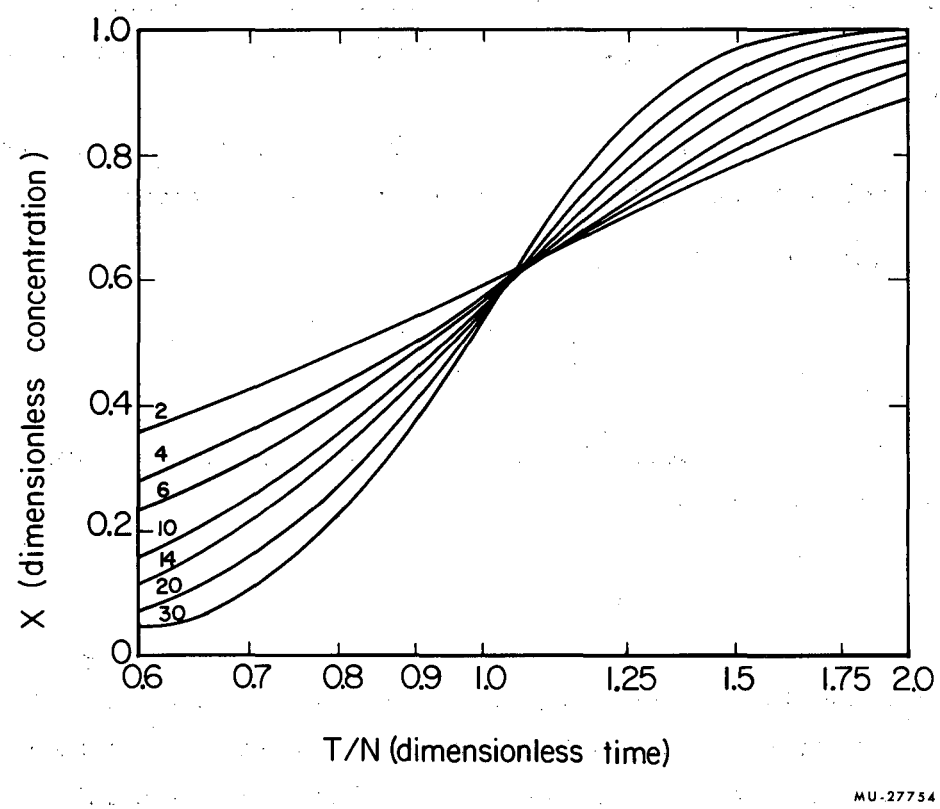

Fig. 2. Random-Walk-model breakthrough curves.

where

C_i = concentration of ith phase,
Z = dimensionless distance along diffusion path,
T = dimensionless time,

and

N_i = column Péclet number of ith phase,

subject to the boundary conditions:

$$T = 0, \quad Z = 0, \quad C_i = 1, \tag{5}$$

$$T = 0, \quad Z > 1, \quad C_i = 0' \tag{6}$$

$$Z = 0, \quad C_i = 1 = \frac{\partial C_i}{\partial Z}; \tag{7}$$

and

$$Z = 1; \quad \frac{\partial C_i}{\partial Z} = 0, \quad C_i = 0. \tag{8}$$

Miyauchi[6] has obtained the solution

$$C_i = \sum_{n=0}^{\infty} \frac{N_i \mu_n [N_i \sin\mu_n Z + 2\mu_n \cos\mu_n Z]}{\left[\left(\frac{N_i}{2}\right)^2 + N_i + \mu_n^2\right]\left[\left(\frac{N_i}{2}\right)^2 + \mu_n^2\right]} \exp\left[\frac{N_i Z}{2}\left\{1 - \frac{T}{N_i Z}\left(1 + \frac{4\mu_n^2}{N_i^2}\right)\right\}\right], \tag{9}$$

where μ_n is given by the transcendental relation

$$\mu_n = \cot^{-1}\left(\frac{\mu_n}{N_i} - \frac{N_i}{4\mu_n}\right). \tag{10}$$

This solution is restricted for $Z \ll 1$. For a detailed treatment of the development of these boundary conditions the reader is referred to Miyauchi.[6]

A graphical presentation of the solution is given in Fig. 3, a semilog plot of dimensionless concentration vs log dimensionless time. Again, the time scale is normalized about the stoichiometric time.

Midpoint slopes of the diffusion-model breakthrough curves were determined by replotting the data of Fig. 3 on rectangular paper and measuring the midpoint slopes. These slopes were calculated based on a time scale of $t_{(x=0.5)} = 1$. Results are expressed in Fig. 4, where the log of the column Péclet number is plotted against the midpoint slope. For comparison, the correlation for the random-walk model as obtained from Eq. (3) is also shown in this plot.

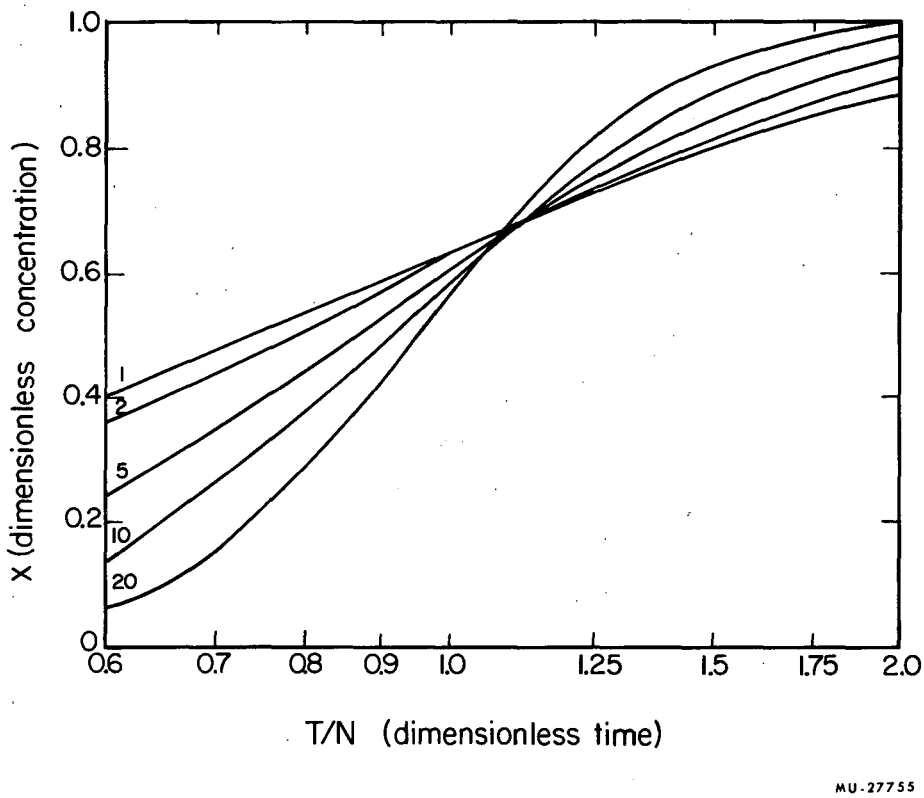

Fig. 3. Miyauchi diffusion-model breakthrough curves.

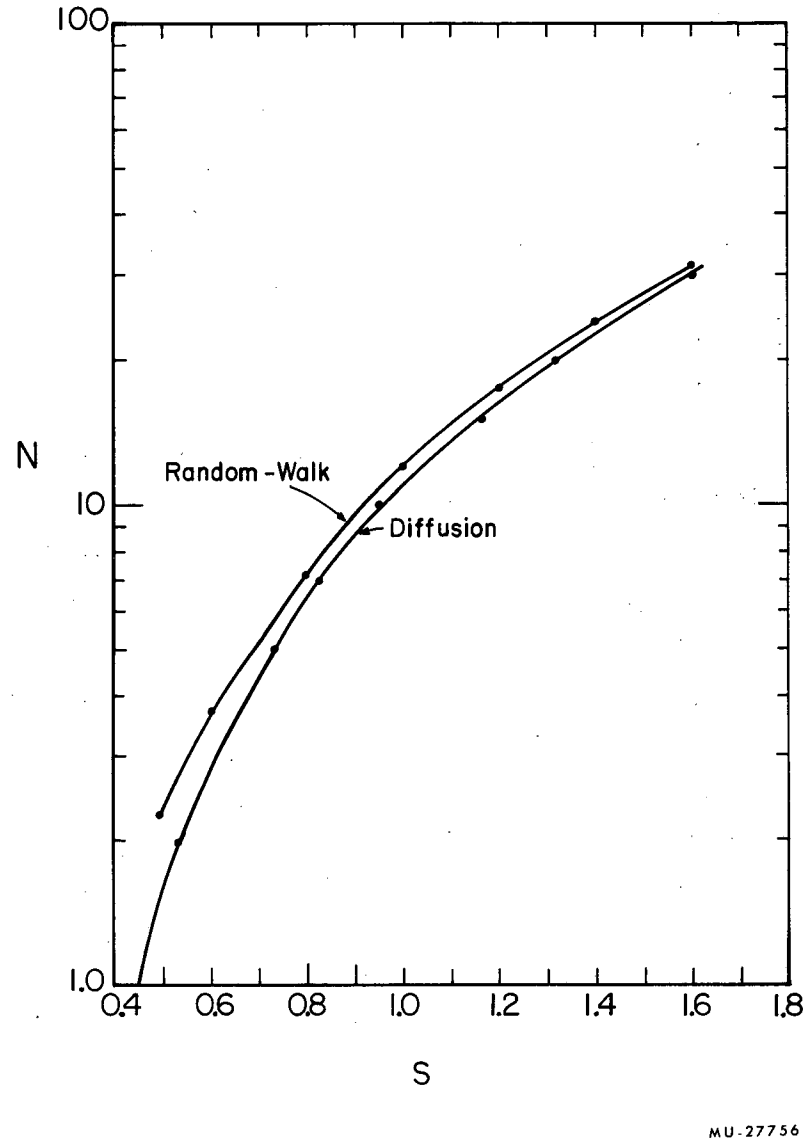

Fig. 4. Midpoint slope correlation for diffusion model and Random-Walk model.

EXPERIMENTAL PROCEDURE

Apparatus

A more detailed description of the apparatus may be found in the thesis of T. T. Word.[13] The gas-absorption column is diagrammed schematically in Fig. 5. The heart of the apparatus was a 2-ft-diam column divided into three flanged sections: (a) a 3-ft-long top section which served the liquid-feed and de-entrainment functions, (b) a 6-ft-long packed section, and (c) a 4-ft bottom section used as a liquid reservoir and gas-entry port.

A 20-hp blower was used to supply air to the tower. A once-through flow of air was found expedient. It was necessitated by tracer buildup which complicated the analysis of gas breakthrough curves, when air was recycled in a closed loop; it eliminated the use of steam coils and water cooler originally provided. Flow rates were measured by an air-impact nozzle, located upstream of the blower and connected to draft-gage manometers.

Liquid was recycled from the water reservoir through a centrifugal pump to the water-feed distributor in the top section. Flow rates were measured either by a 2-15/16-in. orifice located in a 4-in. line or by a 1.25-in. orifice in a 2-in. line. Orifice pressure drops were displayed on a manometer.

The tracer injected into the bulk-water phase was an aqueous solution of 0.3M to 1M sodium nitrate. A schematic diagram of this system is shown in Fig. 6. A portion of the sodium nitrate solution was recycled through a centrifugal pump to a 55-gal storage tank. A side stream was withdrawn from the pump discharge, through a filter and rotameter; the stream was either returned to the storage tank or fed into the column through an injection manifold, the choice being controlled by the setting of a three-way solenoid valve.

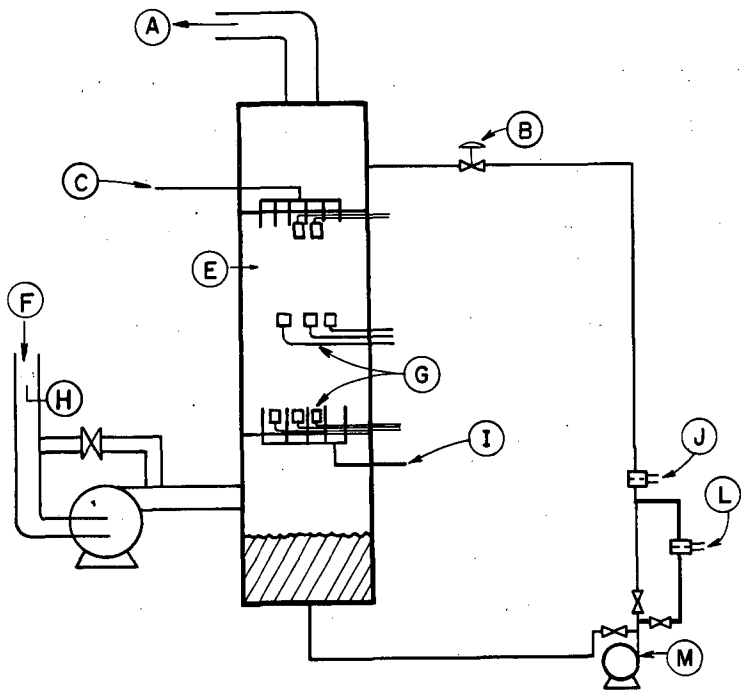

MU-27757

Fig. 5. Schematic diagram of apparatus: A-air discharge, B-pneumatic valve, C-sodium nitrate tracer injection, D-gas-sampling cells, E-packed section, F-air intake, G-liquid-sampling cells, H-air-impact nozzle, I-helium-tracer injection, J-2.938-in. orifice, K-blower, L-1.25-in. orifice, M-liquid pump.

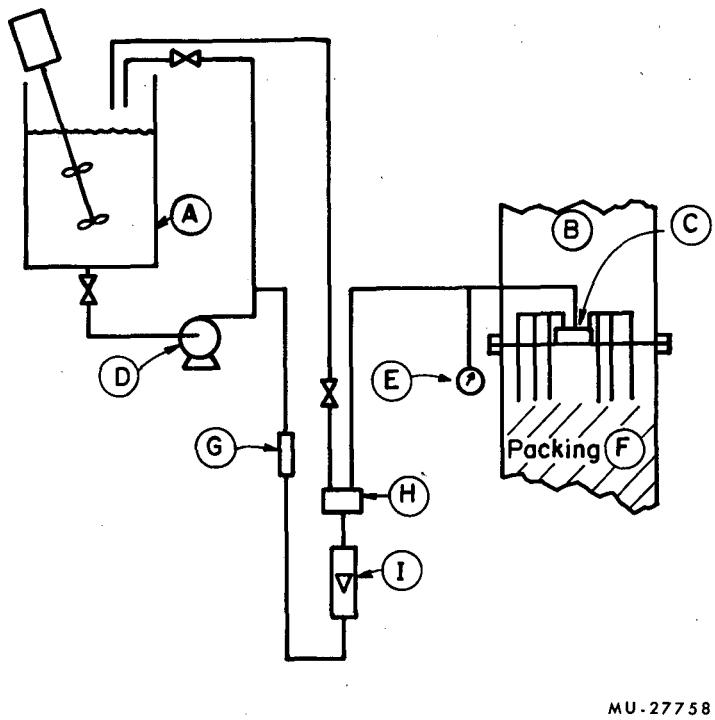

Fig. 6. Flow diagram of liquid-tracer injection system: A-55-gal tracer storage tank, B-top section, C-liquid-tracer manifold, D-centrifugal pump, E-pressure gauge, F-packing, G-filter, H-three-way solenoid valve, I-rotameter.

Performance of the liquid-tracer injection manifold first used was unsatisfactory. The trouble was traced to the formation of an air pocket in the manifold that gave rise to surges and uneven distribution of tracer flow through the sixteen takeoff legs. It was important that the injection conform closely to a step input and be evenly distributed across the column cross-section. Consequently, a second manifold was constructed (see Fig. 7). The air-pocket problem was eliminated by arranging the takeoff legs on the top of the reservoir, rather than on the sides. In addition, the reduction of the diameter of the legs to 0.09375 in. caused the flow to distribute quite evenly among all 16 legs.

A pressure gauge was installed on the line leading to the manifold to indicate the injection behavior. When the three-way solenoid valve was energized and flow to the manifold had begun, a slight delay was observed; then the gauge rose rapidly to a steady value. The delay was caused by the filling of the line to the manifold, which drained each time the solenoid was de-energized. Observation of the pressure gauge indicated that the tracer flow rate did approximate a step function satisfactorily; the precise moment when flow began could be determined by noting the instant the gauge responded.

The tracer used for the air phase was a stream of helium. The helium-tracer injection system is shown schematically in Fig. 8. Helium flow to the column was initiated by pressurizing the surge tank with helium, and opening a three-way solenoid valve to the gas-tracer injection manifold. This manifold consisted of 26 injection tubes distributed over the column cross-section, as shown in Fig. 9. Flow to the manifold was stopped abruptly by opening the two-way solenoid to the atmosphere, then de-energizing the three-way solenoid. This latter action simultaneously shut off flow to the manifold, and opened the manifold to the atmosphere. Discontinuance of gas tracer approximated a step function more closely than tracer startup, so all gas breakthrough curves taken were for the tracer-purging step.

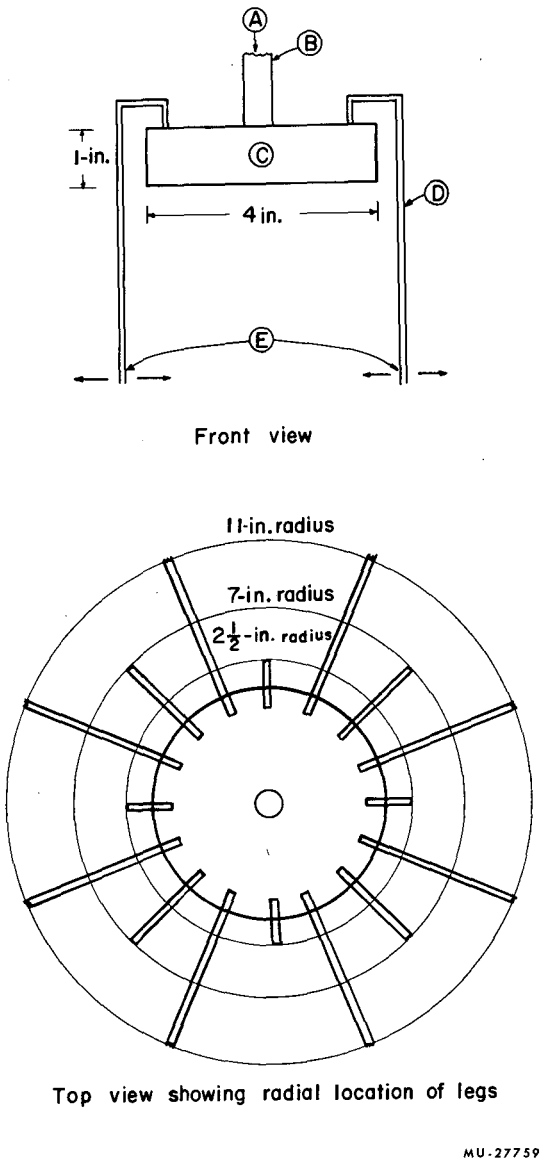

Fig. 7. Liquid-tracer injection manifold: A-tracer inlet, B-0.5-in. o. d. tubing, C-reservoir, D-16 legs 0.09375-in. o. d., E-tracer outlet through 0.03125-in. holes.

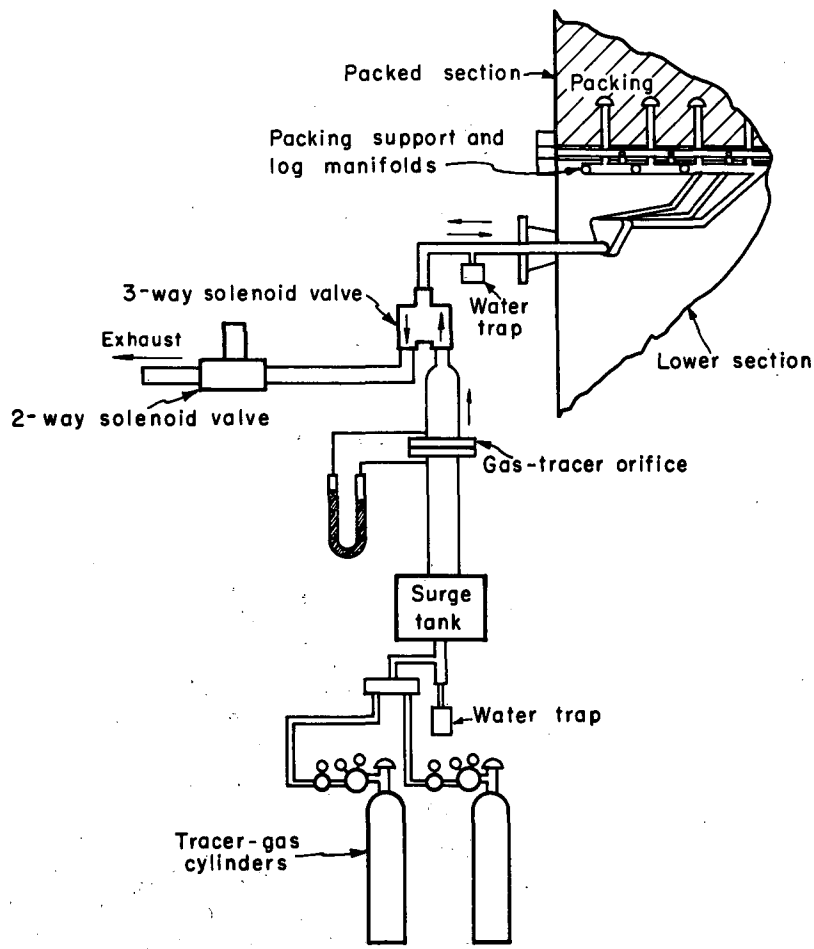

MU-24349

Fig. 8. Schematic diagram of the gas-tracer injection system.

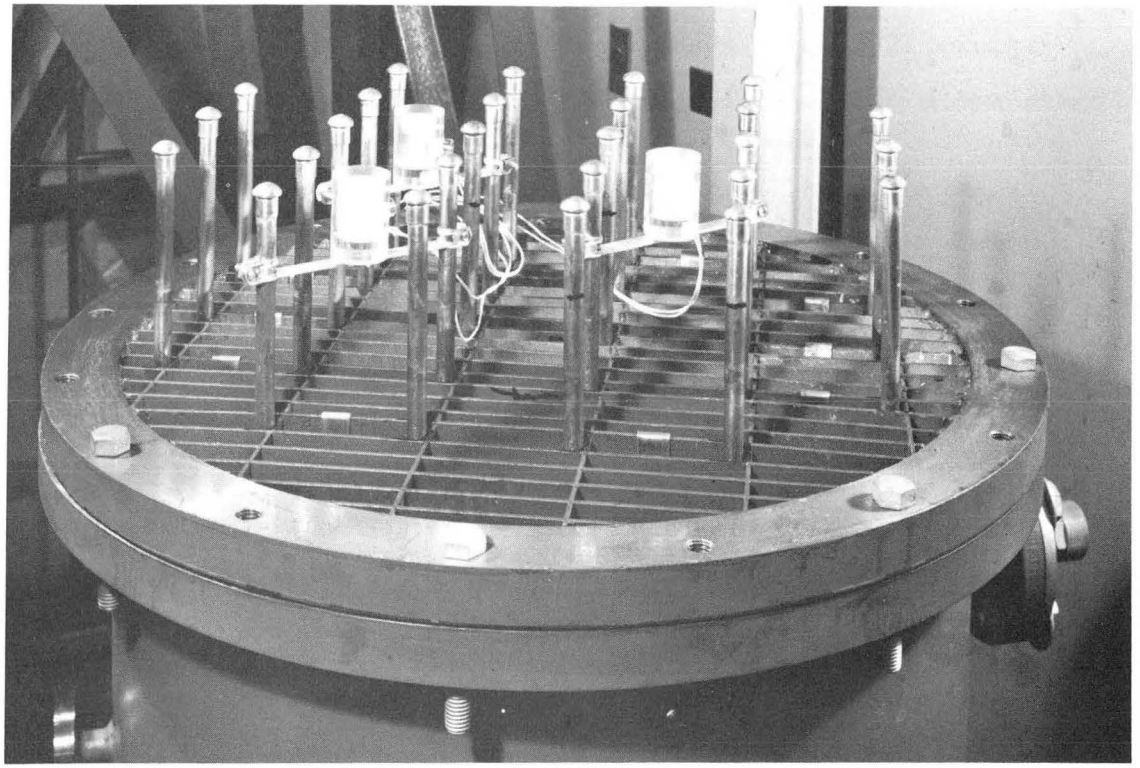

ZN-2875

Fig. 9. Gas-tracer injection manifold.

Sodium nitrate concentration was continuously monitored downstream by means of an electrical-conductivity measurement. Three conductivity cells were located midway down the packed section, and three more at the base of the packed section. A photograph of a sampler is shown in Fig. 10 and a cross-sectional drawing is shown in Fig. 11. These samplers are also shown in position at the base of the tower in Fig. 9. Liquid entered the samplers through the funnel-shaped top and left through the port in the side. A high-frequency voltage (approx 300 at 1000 cps) was impressed across two rhodium-plated nickel-pins electrodes which were kept submerged in fluid to give a continuous reading. The conductance of the solution between the pins was determined by amplifying and recording the output signal. A two-channel amplifier provided simultaneous measurement of liquid conductivity at two points in the column. The recorder chart could be marked to denote the beginning of tracer flow by tripping an external switch connected to one of the channels.

To determine the lower limit of liquid flow rate to which the samplers would respond, flow through a sampler was observed outside the column. An experiment was assembled in which column conditions were simulated, and satisfactory operation of the samplers could be observed if the liquid flow rate was maintained above 1000 lb/hr-ft^2. Consequently, no runs were made for L values less than 2000 lb/hr-ft^2.

As a final check on the electrical-conductivity measuring system, solutions of known relative sodium nitrate concentration were prepared and placed in a liquid sampler, and the recorder response noted. The absolute concentrations were in the range used for experimental runs. The recorder response vs sodium nitrate concentration was truly linear for both channels, as shown in Fig. 12. Since the water used in all experiments had a finite conductivity at zero sodium nitrate concentration and no bias was subtracted, the curve is not expected to pass through the origin.

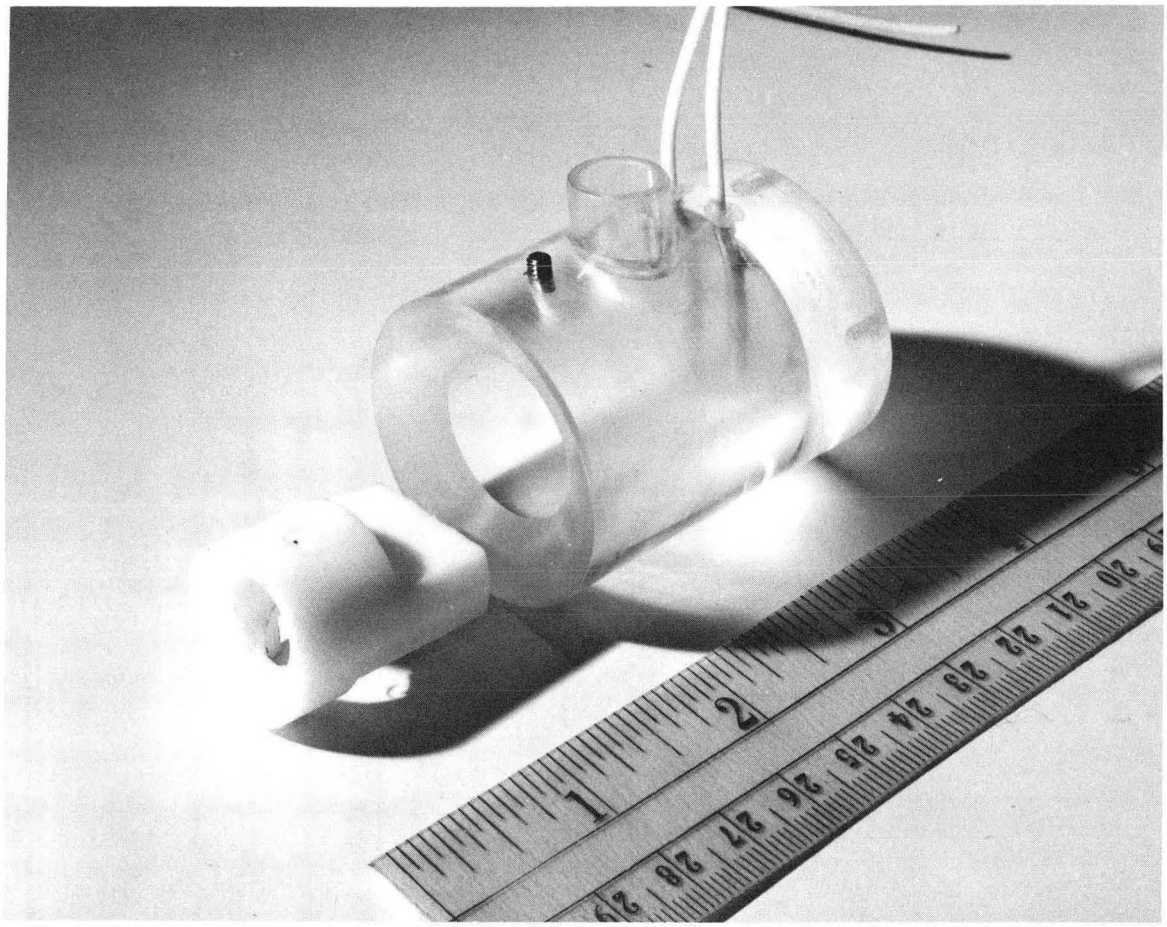

ZN-2876

Fig. 10. Liquid-conductivity cell.

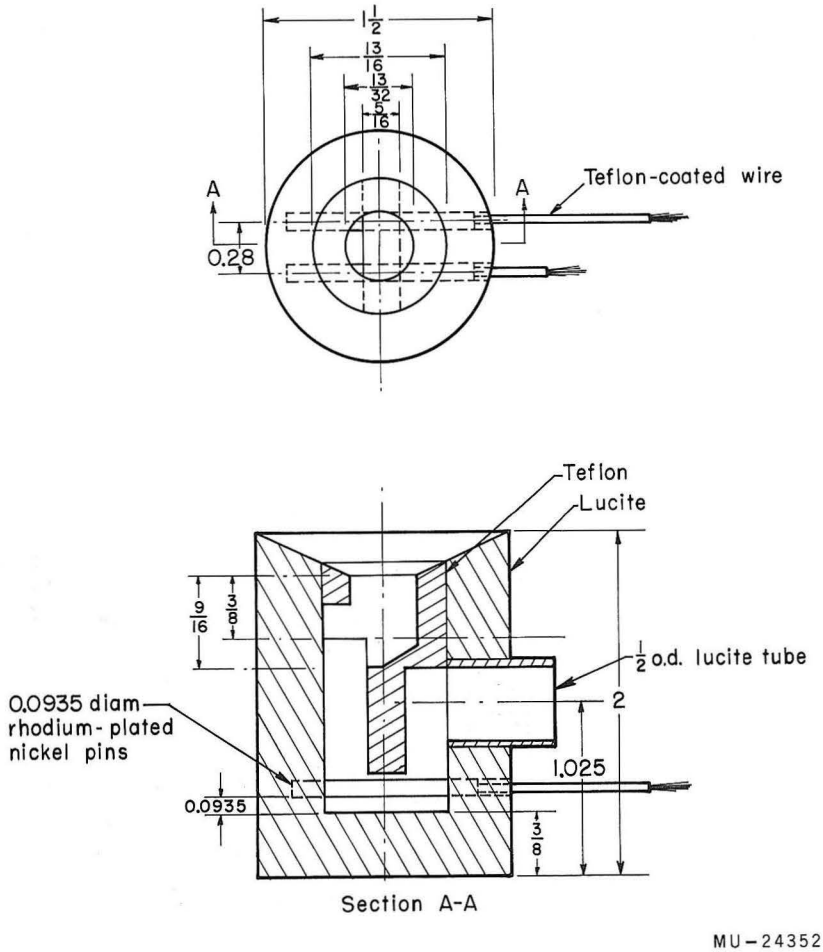

Fig. 11. Cross-sectional drawing of a liquid-conductivity cell.

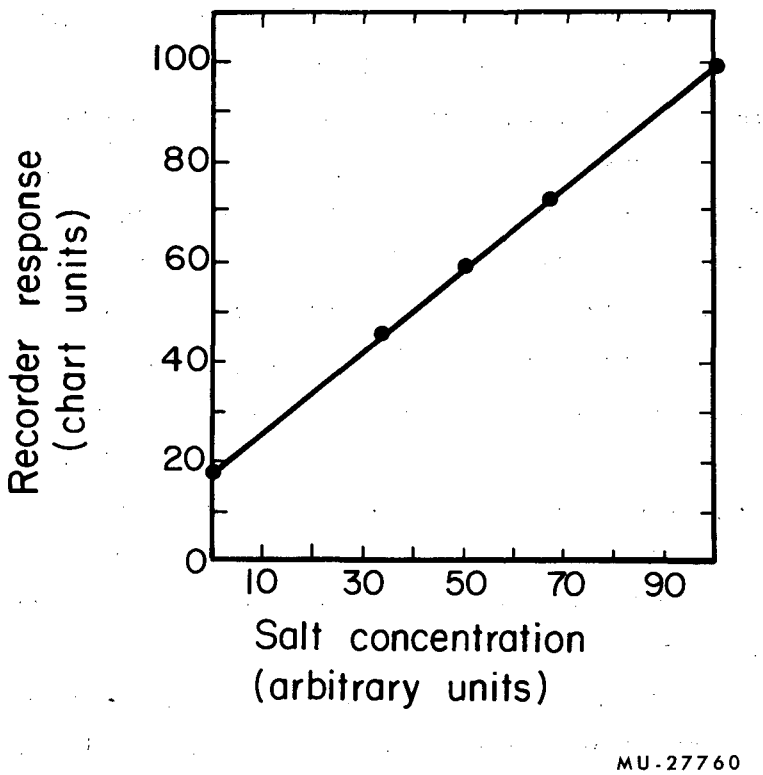

Fig. 12. Liquid-conductivity calibration.

Helium tracer was detected only at the top of the packed section by either of two gas samplers. A vacuum system provided suction for flow through either gas sampler to a thermal-conductivity cell used to measure helium concentration. A diagram of the thermal-conductivity cell is shown in Fig. 13. A dc voltage was impressed across an extremely fine (0.45-mil-diam) tungsten wire which thus became heated to a certain temperature. The heat transfer, hence the temperature of the wire, depends in part upon the thermal conductivity of the gas stream flowing past the wire. This wire was incorporated in a Wheatstone-bridge circuit as shown in Fig. 14. The wires resistance, which is dependent on temperature, was measured indirectly by amplifying and recording the out-of-balance voltage of the bridge circuit relative to a null position. Further, the low sensitivity of the bridge circuit made if necessary to install a preamplifier ahead of the Brush amplifier (shown in Fig. 14) which could be used to boost the signal by a factor of ten.

The recorder response was linear with respect to the helium concentration flowing through the cell (see Fig. 15). As in the case of the liquid recorders, an external switch was provided to mark the start or end of injection on the recorder chart.

Two gas samplers (1-A and 1-B) were constructed [13] (see Fig 16). They were cylindrical in shape with a protective cage enclosing the porous Teflon disk through which the gas sample was withdrawn. The sampler volume downstream of this porous Teflon plug was minimized to reduce back-mixing in the gas entering the thermal-conductivity cell. During column operation the samplers provided a steady-flow sample of gas to the thermal-conductivity cell.

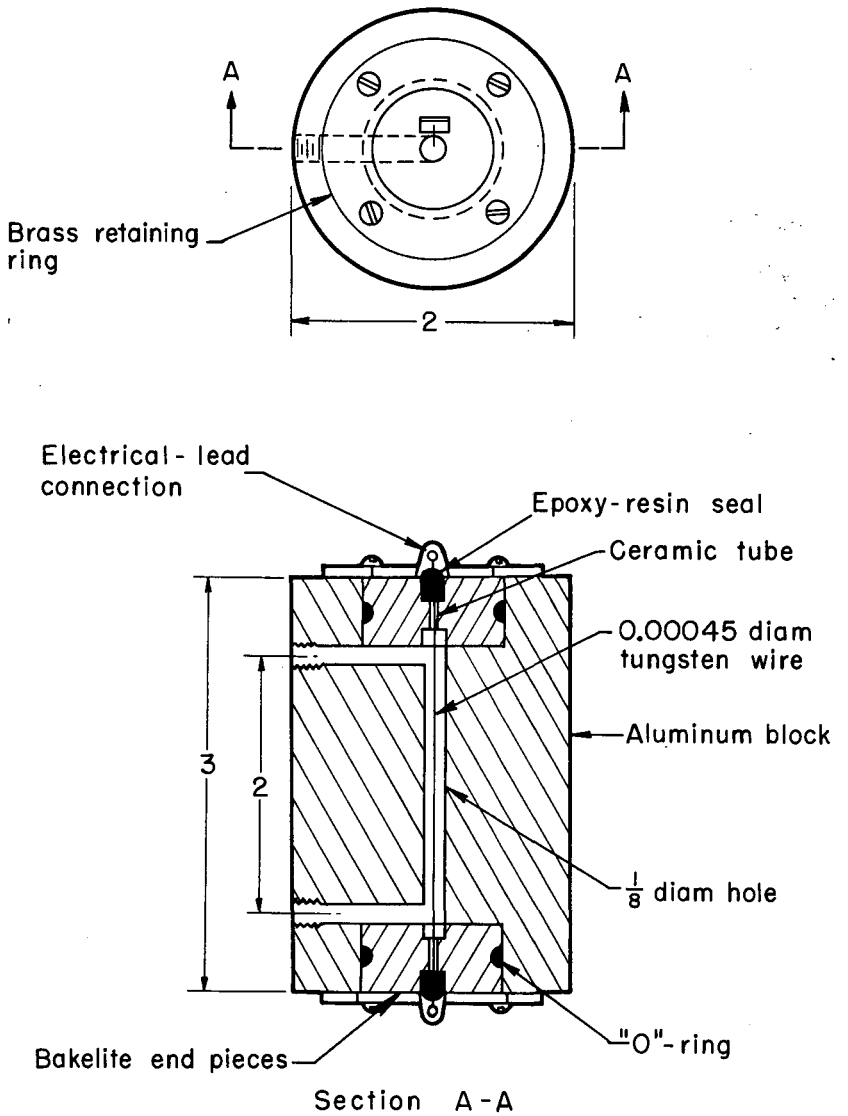

Fig. 13. Cross-sectional drawing of a thermal-conductivity cell.

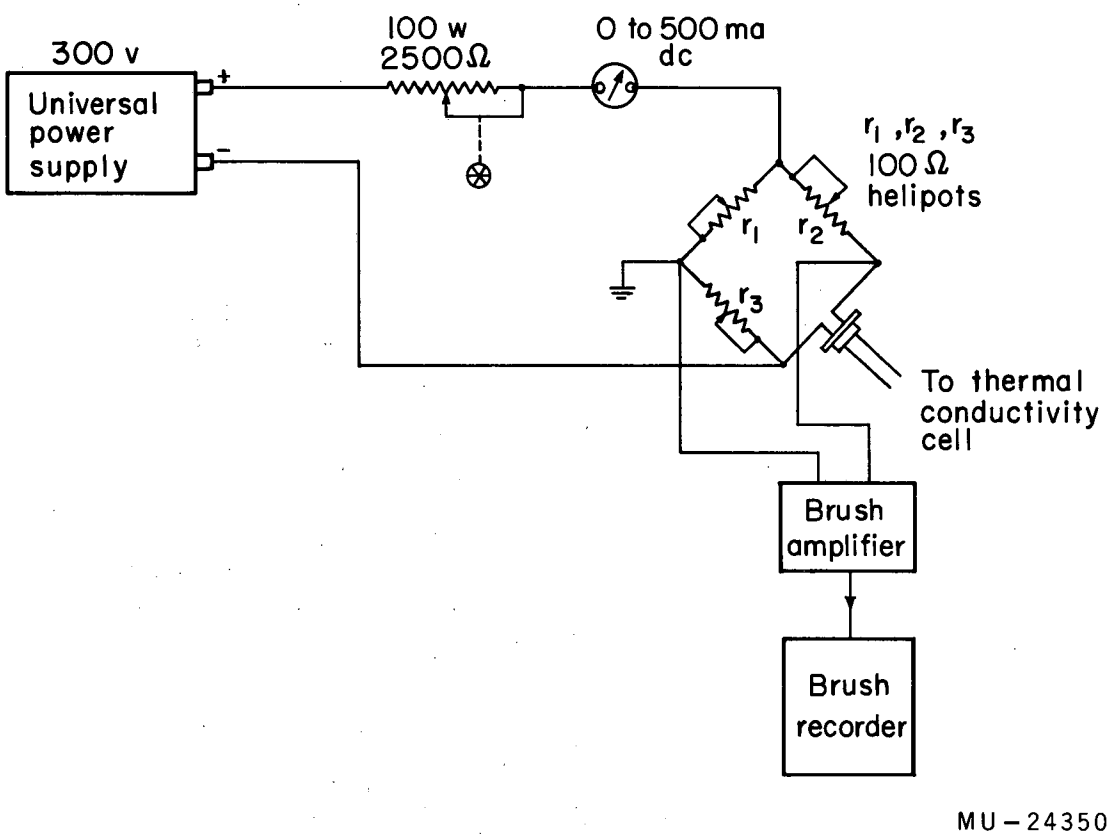

Fig. 14. Wiring diagram for the thermal-conductivity recording and amplifying system.

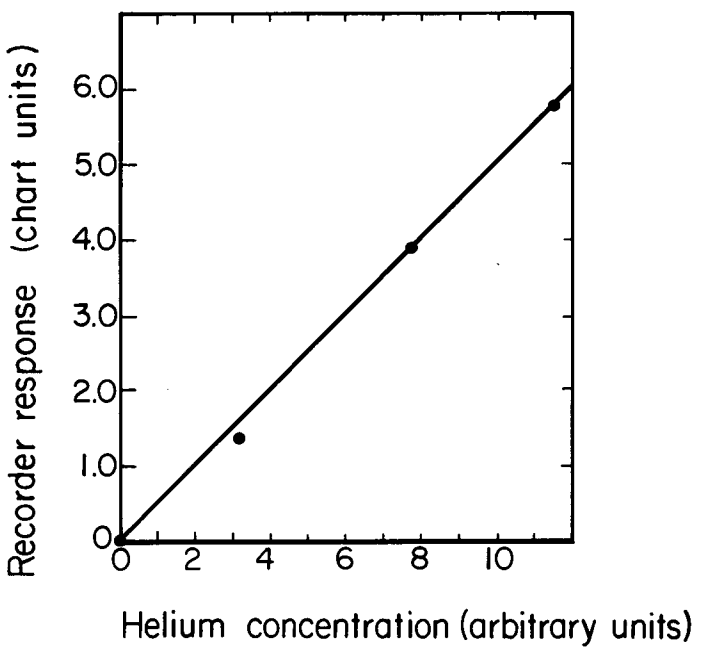

MU-27761

Fig. 15. Helium thermal-conductivity calibration.

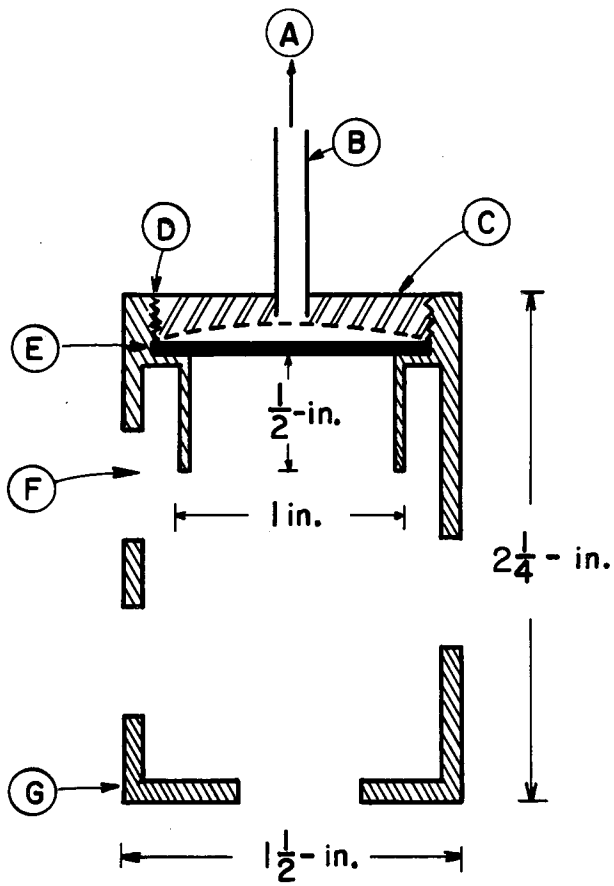

Fig. 16. Detail of gas sampler: A-gas sample, B-0.125-in. o.d. tube, C-screw cap, D-seal formed with waterproof tape, E-porous Teflon, F-0.5-in. drilled holes, G-protective cage.

Procedure

Runs were made at liquid flow rates of 2000, 5000, 8000, and 11000 lb/hr-ft^2, and the gas rate was increased until either flooding or excessive entrainment of water overhead was encountered.

The following method was used to measure breakthrough. First the liquid and gas rates are adjusted to the desired values, and the column brought to steady-state operation. The liquid-conductivity amplifier gains are adjusted so that approximately full-scale deflections would be obtained. The liquid-conductivity recorder chart is started, and the sodium nitrate tracer flow (about 1% to 4% of the total flow) was begun by activating the solenoid valve to the liquid-tracer manifold. A mark is made on the chart by the external switch when liquid-tracer flow first begins, as indicated by pressure gauge on the liquid-tracer manifold. After the two traces have been obtained, the tracer concentration in the recycling liquid is reduced by opening a drain valve and a water-makeup line simultaneously, adjusting the latter manually to maintain a constant liquid level in the water reservoir. By this method, traces were obtained for all six liquid samplers.

For gas-phase measurements, the suction head is adjusted to give the prescribed sampling rate. One balances the bridge circuit by first noting the recorder's null position when a shorted phone plug is inserted in the amplifier-input jack, by connecting the bridge to the amplifier input and adjusting the variable resistance to give a null-position recorder reading. Amplifier gain is adjusted to give approximately the desired full-scale deflection. Helium flow to the column, about 3 mole % of the air and flow, is started and the recorder turned on. Then the chart is marked to denote the beginning of a purging run, as the helium flow is stopped.

After six liquid traces and two gas traces had been obtained at the same L and G values, the liquid holdup in the column was measured. To do this, the pneumatic valve in the liquid-feed line was closed the liquid-level rise in the reservoir was observed as the water in the packing drained into the reservoir.

The gas rate was then increased, and the entire procedure repeated until a further increase in gas rate caused flooding or excessive entrainment. Because of the relatively poor precision of the data, especially for the liquid, all runs were repeated a second time; thus, in general, 12 liquid traces and 4 gas traces were available for a given set of flow rates.

A time delay occurred in transporting gas from the sampler in the column, through a 1/16-in. i. d. tube about 3 ft long to the thermal-conductivity cell. This dead time was measured for each separate column packing. With the column disassembled, the gas samplers were exposed by removing the top 6 in. of packing. Flow through the sampler was set to the prescribed rate, the bridge was balanced as before, and the recorder was started. A hypodermic syringe was filled with helium and discharged at the mouth of the sampler; the time interval from discharge to response was noted on the recorder chart.

Packing Characteristics

The void fraction, ϵ, was measured for all packings used: the 1-in. Raschig rings, the 1-in. Berl saddles, and the 2-in. Raschig rings. The surface area per unit volume, a_p, was measured for the 1-in. and 2-in. Raschig rings.

For the 1-in. and 2-in. Raschig rings, which were a standard geometric shape, these packing characteristics were determined by measuring the dimensions of representative samples of the packing with calipers, by counting the number of particles per unit volume, and by calculating ϵ and a_p.

The void fraction of the 1-in. Berl saddles was obtained by packing a large container of known volume with the saddles and measuring the amount of water necessary to fill the voids.

Equivalent diameter of the packing was reported as the diameter of a sphere with the same surface-to-volume ratio as a packing

particle. From the properties of a sphere,

$$d_p = \frac{6(1-\epsilon)}{a_p} .$$

For these experiments as well as for the runs, the packing was "dry-packed, unshaken." Results are shown in Table I.

Table I. Packing characteristics.

Packing	ϵ	a_p (ft^2/ft^3)	d (in.)
1-in. Raschig rings	0.682	60.8	0.376
2-in. Raschig rings	0.690	29.8	0.749
1-in. Berl saddles	0.740	79(Ref. 12)	0.237

RESULTS AND CONCLUSIONS

For all three column packings studied, the gas data seemed to be correlated fairly well by the random-walk mixing model. Midpoint slopes were computed for all gas runs, and the column Péclet number determined from Eq. (3). Values for breakthrough time at $x = 0.5$ were based on a corrected time scale which took into account the dead time of the gas-sampling system. Packing Péclet numbers were computed by multiplying the column Péclet number by d_p/h. Pertinent data are summarized in Tables IV through VI in the Appendix. A sample calculation is given on the first page of the Appendix.

Results for all packings used are shown graphically in Figs. 17, 18, and 19, where packing Péclet number is plotted on a logarithmic scale vs liquid flow rate on a linear scale, with gas flow rate as the parameter. Reproducibility of the data was fairly good, with mean deviations of 10% being typical.

As evidenced by the plots, the degree of mixing in the gas phase was found to increase with both liquid and gas flow rates. The dependence of Péclet number upon flow rate was more pronounced for the 1-in. Raschig rings and 1-in. Berl saddles than for the 2-in. Raschig rings. Results may be expressed empirically as follows for the ranges $0 \leq L \leq 11{,}000$ lb/hr-ft^2 and $300 \leq G \leq 1100$ lb/hr-ft^2:

for 1-in. Berl saddles,

$$P = (0.822 - 4.73 \times 10^{-4} G)\, 10^{-3.85 \times 10^{-5} L}; \tag{11}$$

for 1-in. Raschig rings,

$$P = (0.665 - 3.83 \times 10^{-4} G)\, 10^{-3.85 \times 10^{-5} L}; \tag{12}$$

and

for 2-in. Raschig rings,

$$P = (0.756 - 1.875 \times 10^{-4} G)\, 10^{-1.61 \times 10^{-5} L}. \tag{13}$$

Table IV. Summary of gas-phase Péclet numbers, 1-in. saddles

L	G	Sampler 1-A		Sampler 1-B			$\overline{N}$	% dev	P
0	300	160	190	160	(260)[a]	175	171	6	0.68
0	500	145	94	97	122		115	17	0.45
0	700	120	135	94	150		125	15	0.49
0	900	120	120	150	94		121	12	0.48
0	1100	91	77	81	72		80	8	0.32
2,000	300	140	140	140	145		141	1	0.56
2,000	500	130	100	140	125		124	10	0.49
2,000	700	92	115	105	96		102	8	0.40
2,000	900	73	63	60	79		69	10	0.27
2,000	1100	65	62	60	52		60	7	0,24
5,000	300	160	125	92	130		127	14	0.50
5,000	500	88	99	125	94		102	12	0.40
5,000	700	77	78	82	96		83	7	0.33
5,000	900	66	78	76	61		70	10	0.28
8,000	300	66	89	75	115		86	19	0.34
8,000	500	63	66	77	78		71	7	0.28
8,000	700	66	89	56	81		73	16	0.29
11,000	300	65	47	65	52		52	13	0.21
11,000	500	51	66	64	61		61	10	0.24

[a] Numbers in parentheses indicate they have not been included in the final average.

Table V. Summary of gas-phase Peclet numbers, 1-in. rings.

0	300	82	99	94	78					88	10	0.55
0	500	59	59	55	60	68	58	59	65	60	5	0.38
0	700	40	71	52	57					55	16	0.34
0	900	(77)[a]	55	55	58					56	2	0.35
0	1100	35	40	28	37					35	10	0.22
2000	300	82	68	72	69					73	7	0.46
2000	500	49	52	60	57					55	7	0.35
2000	700	50	60	63	48	39				52	15	0.33
2000	900	42	42	55	39					45	12	0.28
5000	300	44	54	47	51	47	46			48	6	0.30
5000	500	36	54	35	33	44	43	41		41	13	0.26
5000	700	31	38	32	54					39	20	0.24
8000	300	25	47	33	22	25	52	29	37	34	26	0.21
8000	500	32	40	41	32	49	34			38	14	0.24
11000	300	39	33	42	45					40	9	0.25

[a]Numbers in parenthesis indicate they have not been included in the final average.

Table VI. Summary of gas-phase Péclet numbers, 2-in. rings

G	<	Sampler 1-A		Sampler 1-B		$\bar{N}$	%dev	P
300	0	58	44	57	62	55	10	0.69
500	0	40	58	47	50	49	11	0.61
700	0	47	47	31	66	48	19	0.60
900	0	57	47	40	39	46	14	0.57
1100	0	42	42	50	40	44	8	0.55
300	2,000	64	62	(48)[a]	60	62	2	0.77
500	2,000	55	46	46	55	51	9	0.64
700	2,000	44	42	45	47	45	3	0.56
900	2,000	47	54	45	52	50	7	0.62
1100	2,000	51	37	40	36	41	12	0.51
300	5,000	(25)	43	37	47	42	9	0.52
500	5,000	41	36	35	40	38	7	0.47
700	5,000	42	42	40	49	43	7	0.54
900	5,000	42	29	38	35	36	11	0.45
1100	5,000	38	39	32	(52)	36	8	0.45
300	8,000	51	37	40	27	39	17	0.49
500	8,000	20	19	28	36	26	24	0.32
700	8,000	44	28	40	34	37	15	0.46
900	8,000	38	33	45	35	38	10	0.47
1100	8,000	31	29	33	37	33	8	0.41
300	11,000	37	(15)	(20)	37	37	0	0.46
500	11,000	42	17	55	22	34	43	0.42
700	11,000	40	39	25	28	33	20	0.41
900	11,000	40		38		39	3	0.49

[a]Numbers in parentheses indicate they have not been included in the final average.

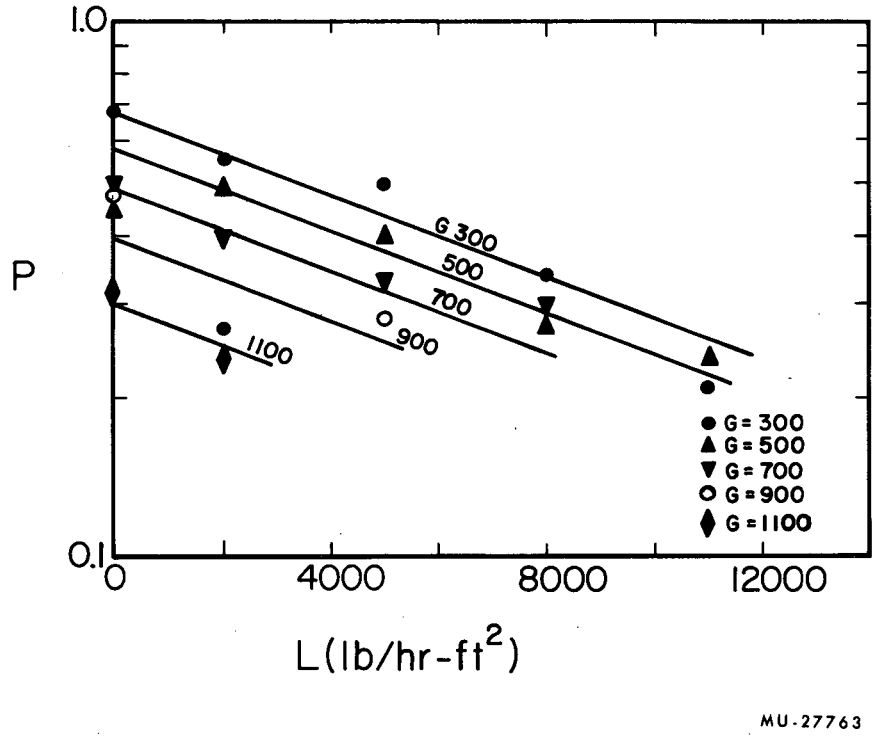

Fig. 17. Gas-phase Péclet numbers, 1-in. Berl saddles.

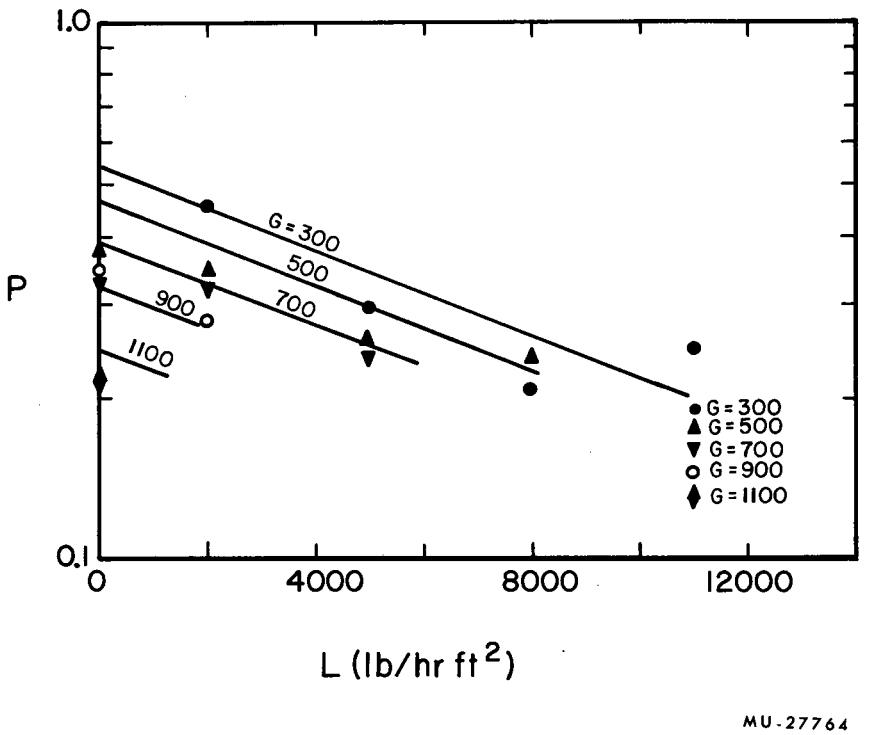

Fig. 18. Gas-phase Péclet numbers, 1-in. Raschig rings.

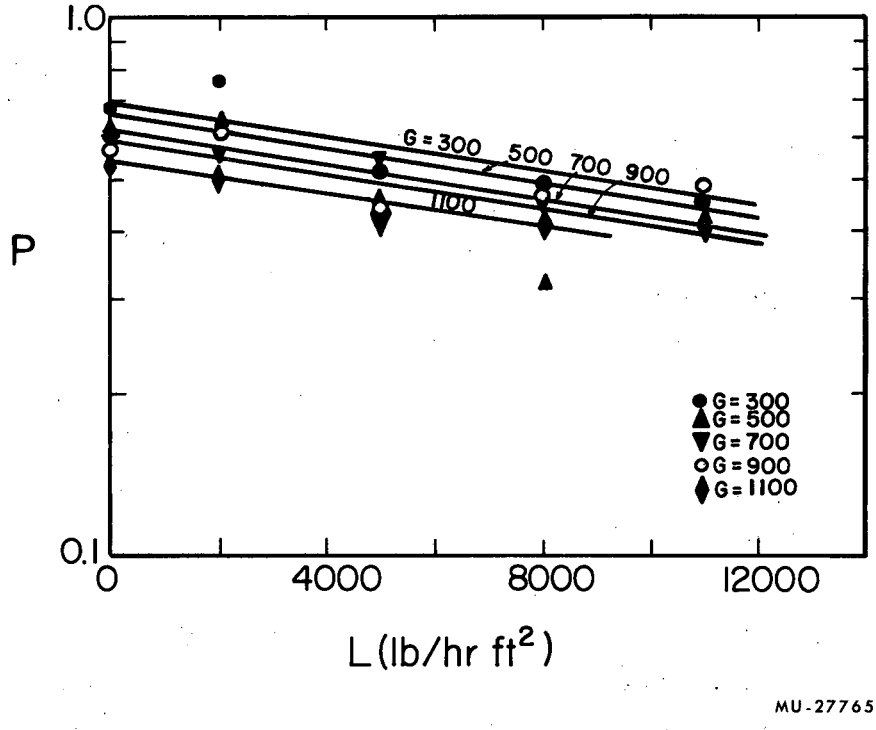

Fig. 19. Gas-phase Péclet numbers, 2-in. Raschig rings.

Liquid-side data were analyzed by the diffusion model. Some of the experimental breakthrough curves were first compared with those predicted by the diffusion, random-walk, mixing-cell, and segmented laminar-flow.[4] None of the models tested fitted the data exactly; however, the diffusion model came the closest.

In determining midpoint slopes for the liquid traces, the time scale was corrected for the dealy time of the sampler; piston flow between the sampler inlet and the electrodes, and uniform flow distribution across the column cross section, were assumed in applying this correction. Compared to the time at $x = 0.5$, this increment was very small indeed. (The gas-sampler time correction was much more significant.)

Column Péclet numbers were determined by the midpoint-slope correlation for the diffusion model as shown in Fig. 4. Essential data are summarized in Tables VII through IX of the Appendix. An "R" preceding a run number designates the red pen that recorded the samplers at 30-in. normal level relative to the injection level and a "B" the black pen that recorded the samplers at the 60-in. level. A sample calculation is presented on page 59 of the Appendix.

Reproducibility of the liquid-phase data was poor and was characterized by mean deviation of 30%. Part of the scatter was undoubtedly caused by the difficulty of determining the slope of the breakthrough curves which sometimes fluctuated erratically in the region of interest, reflecting the actual fluctuations of flow in the column.

Semilogarithmic plots of Péclet number vs liquid flow rate are shown in Figs. 20, 21, and 22. In contrast to the gas-phase results, axial mixing decreases at increasing liquid rates. The quantitative effect of gas-phase flow rate is negligible compared with the scatter of the present data. For the 1-in. Berl saddles, a trend does seem to be established in which the Péclet number increases with gas rate, but this trend tends to be lost or reversed elsewhere.

Table VII. Summary of liquid-data Péclet numbers 1-in. bed saddles

L	G	Samplers 26-in. downstream of injection						Samplers 60-in. downstream of injection						$\bar{P}_6$	% dev
lb/hr-ft^2	lb/hr-ft^2	1	1	2	2	3	3	1	1	2	2	3	3		
2,000	0	0.058	0.061	0.045	0.025	0.024	0.036	0.027	(0.017)[a]	0.053	0.039	0.057	0.057	0.042	28
2,000	300	0.086	0.064	0.036	0.053	0.055	0.036	0.030	0.029	0.055	0.033	0.036	0.045	0.047	29
2,000	500	0.047	0.071	0.093	0.056	0.046	0.025	0.043	0.030	0.032	0.075	0.023	0.037	0.044	28
2,000	700	(0.109)	0.038	0.053	0.042	0.038	0.016	0.031	(0.012)	0.069	0.047	0.035	0.027	0.040	27
2,000	900	0.049	0.072	0.034	(0.100)	0.035	0.027	0.025	0.034	0.067	0.065	0.055	0.036	0.045	33
2,000	1100	0.071	(0.090)	0.057	0.057	0.043	0.042	0.033	0.038	0.045	0.041	0.053	0.033	0.047	20
5,000	0	0.046	0.066	(0.020)	0.059	0.047	0.084	0.034 / 0.059	0.061	0.047	0.083	0.041	0.055	0.057	21
5,000	300	0.036	—	0.069	0.069	0.057	0.085	0.032	0.059	0.057	0.073	0.047	0.061	0.059	20
5,000	500	—	(0.191)	0.051	0.082	0.055	(0.137)	(0.015)	0.051	0.059	0.079	0.053	0.053	0.060	17
5,000	700	(0.155)	(0.137)	0.067	—	0.041	0.065	0.047	0.043	0.055	0.053	0.059	0.055	0.054	13
5,000	900	0.118	0.088	0.079	0.110	0.022	0.110	0.036	0.073	0.053	0.118	0.043	0.055	0.075	37
8,000	0	0.159	0.137	0.063	0.119	0.050	0.096	0.067	0.053	0.075	0.122	0.061	0.079	0.090	34
8,000	300	0.200	(0.319)	0.066	0.123 / 0.141	0.039	0.100	0.079	0.111	0.063	0.130	0.099	0.063	0.101	33
8,000	500	0.100	0.178	0.123	(0.219)	0.091	0.096	0.042	0.069	0.073	0.111	0.079	0.083	0.095	25
8,000	700	0.118	0.150	0.155	0.178	0.052	0.100	0.044	0.103	0.095	0.138	0.083	0.087	0.109	30
11,000	0	0.100	0.118	0.057	0.105	0.096	0.100	0.051	—	0.071	0.067	0.083	0.061	0.083	23
11,000	300	0.200	0.191	0.114	0.081	0.074	0.056	0.083	0.033	0.057	0.079	0.083	0.065	0.093	41
11,000	500	0.132	0.141	0.114	0.100	0.118	(0.035)	0.075	0.055	0.099	0.091	0.087	0.087	0.100	19

[a] Numbers in parenthese indicate they have not been included in the final average.

Table VIII. Summary of liquid Péclet numbers, 1-in. Raschig rings.

L	G	Samplers 30-in. downstream of injection						Samplers 60-in. downstream of injection						$\overline{P}$	%dev
lb/hr-ft^2	lb/hr-ft^2	1	1	2	2	3	3	1	1	2	2	3	3		
2000	0	0.055	0.044	0.058	0.025	0.044	0.024	0.031	0.025	0.046	0.038	(0.091)[a]	0.040	0.040	23
2000	300	0.023	0.032	0.030	0.032	0.030	0.048	0.022	0.037	0.050	0.037	0.060	0.042	0.037	27
2000	500	0.046	0.028	(0.084)	0.037	0.030	0.035	0.037	0.048	0.062	0.044	0.040	0.031	0.040	18
2000	700	0.032	0.053	0.030	0.044	0.030	0.023	0.017	0.055	0.035	0.049	0.038	0.044	0.037	27
2000	900	0.071	0.092	0.078	0.064	0.037	0.064	0.031	0.061	0.035	0.035	0.056	0.042	0.055	29
5000	0	0.025	0.038	---	(0.125)	0.022	0.053	0.061	0.076	0.070	0.103	0.022	---	0.052	43
5000	300	0.025	0.062	0.048	0.100	0.029	0.062	0.064	0.062	0.070	0.101	0.070	0.066	0.064	24
5000	500	0.030	0.083	0.031	0.150	(0.019)	0.106	0.040	0.132	0.088	(0.194)	0.048	0.103	0.082	43
5000	700	0.118	0.076	0.058	0.138	0.062	0.083	0.066	0.101	0.070	(0.188)	0.058	0.110	0.085	27
8000	0	0.151	0.046	0.175	0.085	0.219	0.038	0.132	---	0.113	0.208	0.163	0.062	0.122	40
					0.072						0.132				
8000	300	0.096	0.046	0.118	0.029	0.150	0.028	0.122	0.085	0.219	0.122	0.116	0.082	0.101	40
8000	500	0.126	0.053	0.182	0.065	0.113	0.037	0.157	0.091	0.251	0.175	0.150	0.107	0.131	35
						0.144						0.175			
11,000	0	0.157	0.044	0.182	0.035	0.094	0.032	0.219	0.076	0.239	0.182	0.175	0.088	0.127	52
11,000	300	0.108	0.036	0.144	0.076	0.150	0.044	0.107	0.107	0.200	0.232	0.110	0.088	0.116	37

[a]Numbers in parenthesis indicate they have not been included in the final average.

Table IX. Summary of liquid Peclet numbers, 2-in. Raschig rings

L	G	Liquid samplers 27-in. downstream of injection						Liquid samplers 60-in. downstream of injection						$\bar{P}$	%dev
lb/hr-ft^2	lb/hr-ft^2	1	1	2	2	3	3	1	1	2	2	3	3		
2000	0	0.047	0.088 0.244	---	---	0.069	(<0.028)	0.084	0.038 0.094	---	---	0.131	0.062	0.077	29
2000	300	0.152	0.064	---	---	(<0.028)	(<0.028)	0.041	0.049	---	---	0.034	0.058	0.066	42
2000	500	0.133	0.056	---	---	(<0.028)	(<0.028)	0.039	0.034	---	---	0.043	---	0.060	49
2000	700	0.058	0.045	---	---	(<0.028)	(<0.028)	0.039	0.020	---	---	0.086	---	0.051	36
2000	900	0.053	0.051	---	---	(<0.028)	(<0.028)	0.043	---	---	---	0.066	0.083	0.058	21
2000	1100	---	0.103	---	---	(<0.028)	(<0.028)	0.038	0.028	---	---	0.088	0.069	0.066	39
5000	0	0.135	0.167	---	---	(<0.015)	0.052	0.083	0.096	0.073	0.096	0.054 0.124	0.160	0.120	31
5000	300	0.122	0.225	---	---	(0.028) (0.030)	(0.039)	0.060	0.137	0.088	0.169	0.124 0.111	0.218	0.139	31
5000	500	0.069	(0.304)	---	---	0.092	0.081	0.066	0.122	0.161	0.062	0.193	0.175	0.103	41
5000	700	0.158	0.163	---	---	(0.045)	(0.051)	(0.049)	0.069	0.098	0.058	0.169	0.150	0.120	35
5000	900	0.178	0.086	---	---	(0.028)	(0.030)	0.049	0.118	0.109	0.156	0.107	0.124	0.116	24
5000	1100	---	0.205	---	---	(<0.028)	(0.047)	0.161	0.077	0.084	0.124	0.131	0.175	0.137	27
8000	0	0.128	0.175	---	0.077	---	(<0.028)	0.045	0.120	0.045	0.066	(0.019)	0.109	0.096	39
8000	300	(0.262)	0.122	---	0.081	(0.028)	(0.036)	0.131	0.107	0.068	0.084	0.051	0.088	0.092	23
8000	500	(0.250)	0.128	---	---	(0.041)	(<0.028)	(0.024)	0.156	0.066	0.075	0.090	---	0.103	28
8000	700	0.111	(0.257)	---	---	0.081	0.066	0.021	0.092	0.069	0.161	0.099	0.116	0.100	23
8000	900	0.081	0.152	---	0.227	(0.028)	0.111	0.060	0.043	0.161	0.120	0.161	0.161	0.128	35
8000	1100	0.051	0.225	0.214	0.092	0.060	0.051	0.069	0.137	0.092	0.156	0.122	0.120	0.116	42
11,000	0	(0.401)	0.272	---	---	0.278	(<0.028)	0.237	0.124	0.175	0.066	0.250	0.111	0.190	37
11,000	300	0.214	0.111 0.374	---	---	0.088	0.077	0.379	0.064	0.250	0.084	0.124	0.150	0.173	54
11,000	500	(0.415)	0.133	---	---	0.075	0.094 (0.036)	0.169	0.098	0.137	0.199	0.137	0.099	0.128	24
11,000	700	0.077	0.053 0.053	0.274	---	0.124	0.056	0.111	0.043	0.143	0.059	0.120	0.122	0.115	42
11,000	900	0.199		(1.17)		0.255		0.180		0.250		0.124		0.201	20

[a]Numbers in parenthesis indicate they have not been included in the final average.

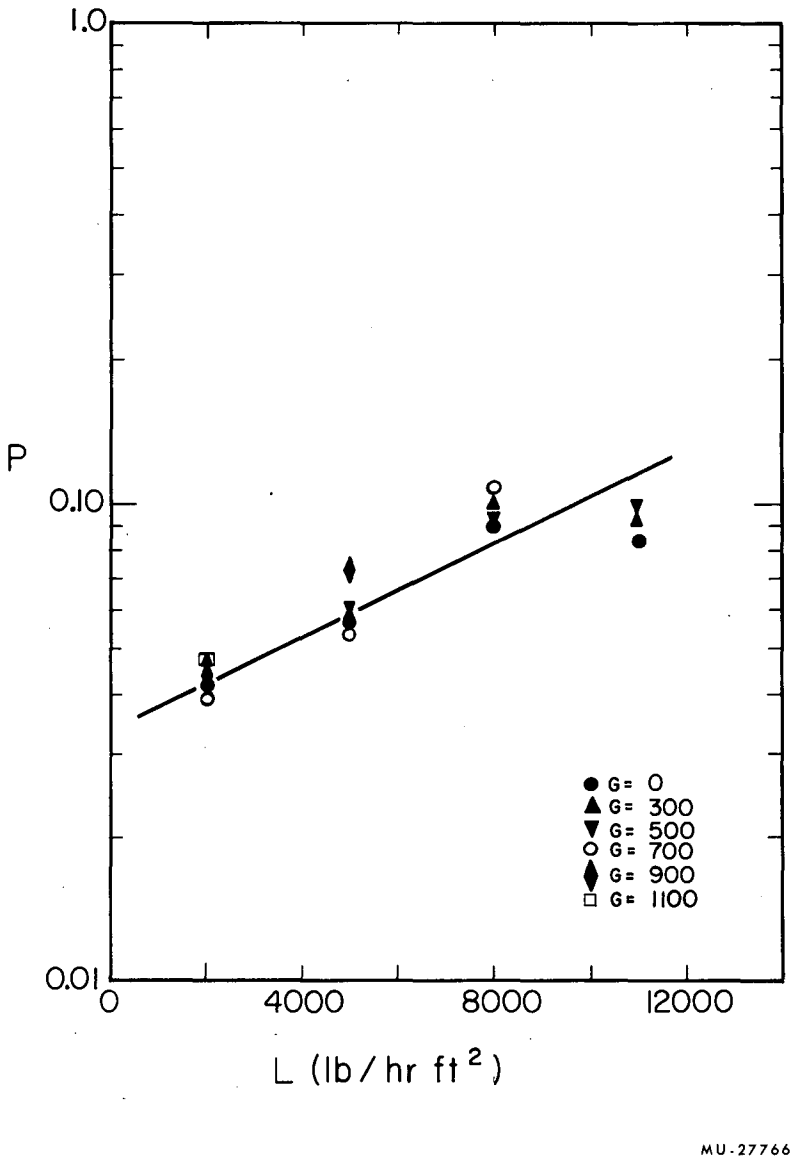

Fig. 20. Liquid-phase Péclet numbers, 1-in. Berl saddles.

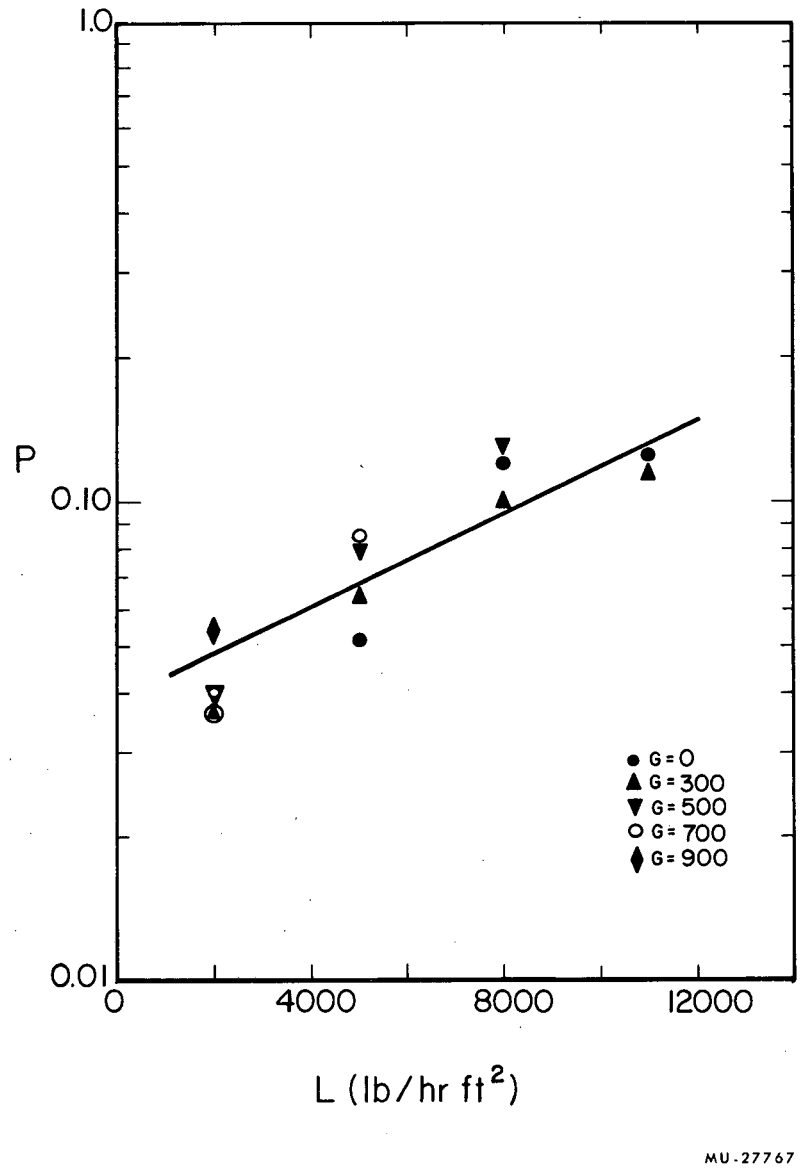

Fig. 21. Liquid-phase Péclet numbers, 1-in. Raschig rings.

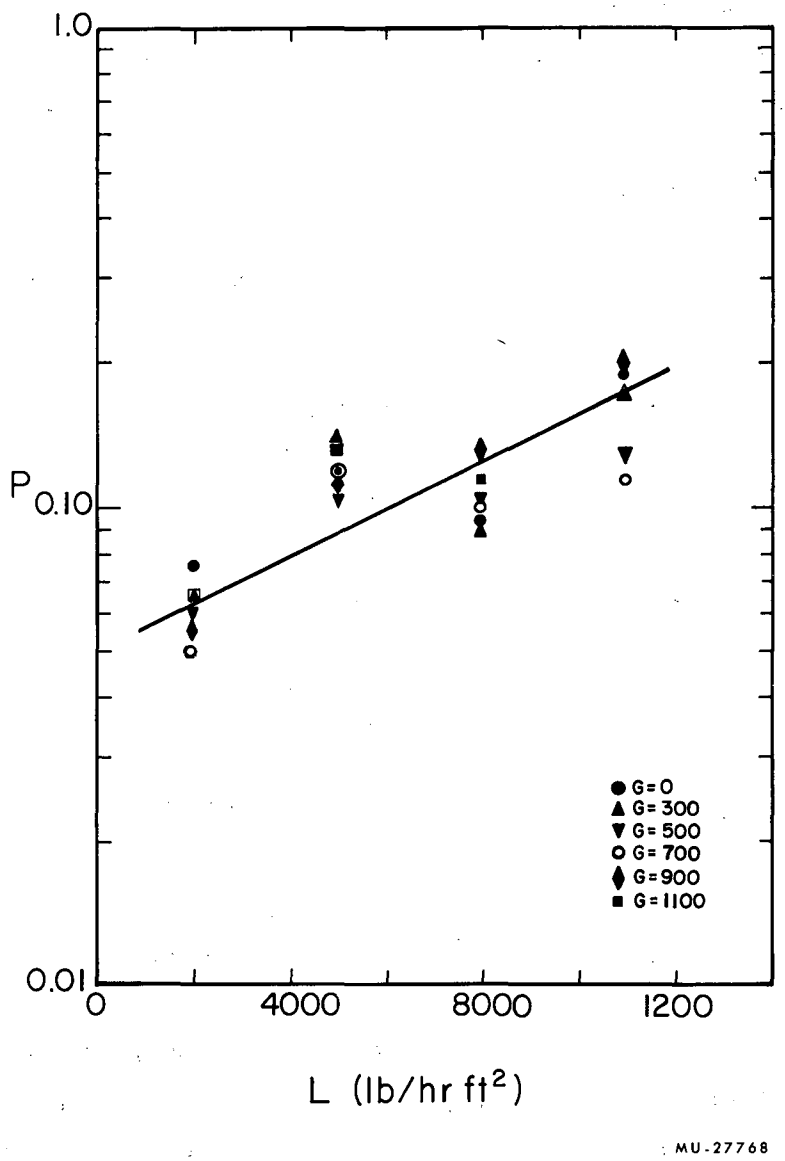

Fig. 22. Liquid-phase Péclet numbers, 2-in. Raschig rings.

For all types of packing studied the dependence of liquid-phase Péclet number on liquid flow rate was found to be approximately the same. The following empirical representation of the data was developed:

for 1-in. Berl saddles,

$$P = (0.033)\ 10^{4.93\times 10^{-5}L}\ ; \tag{14}$$

for 1-in. Raschig rings,

$$P = (0.038)\ 10^{4.93\times 10^{-5}L}\ ; \tag{15}$$

and

for 2-in. Raschig rings,

$$P = (0.051)\ 10^{4.93\times 10^{-5}L}\ . \tag{16}$$

These hold for the range $2000 \leq L \leq 11000$ lb/hr-ft^2, and $0 \leq G \leq 1100$ lb/hr-ft^2.

The straight-line relations drawn in Figs. 20 through 22 represent only one of the possible curves for fitting the data. In all three packings, the slope of log Péclet number against L tends to diminish with increasing L. A log-log plot of Péclet number against L indicated that it would not be unreasonable to represent the relation as a square-root dependence of Péclet number on L. This was the form of correlation developed by Otake and Kunugita.[9]

Another important conclusion is that the extent of mixing in the liquid phase is much greater than in the gas phase. The Péclet number difference is roughly one order of magnitude in the low flow-rate ranges used in these experiments.

In both phases, the Peclet number values obtained correspond to axial-dispersion coefficients in the range of 100 to 200 cm^2/sec; the difference in magnitude of Peclet number between the two phases is offset by a corresponding difference in superficial velocity. Because molecular diffusivity is in the range of 0.7 cm^2/sec and 10^{-5} cm^2/sec for the gas and liquid phases respectively, its contribution to the observed Peclet numbers is negligible. A sample calculation for the dispersion (eddy-diffusion) coefficient is given on page 62 of the Appendix.

A liquid mixing length (E/u) of approximately 7 nominal packing diameters was computed for the typical run given in the Appendix. This was slightly lower than the 10-to-30 range computed from the data of Stemerding[11] but of the same order of magnitude. Stemerding's flow-rate range was considerably less than the one used in this study.

APPLICATION TO DESIGN

Miyauchi and co-workers have developed a practical calculation method for extraction systems in which N_{oxP}, the number of over-all transfer units based on a piston-flow model (e.g., calculated by the Colburn equations) may be related to N_{ox}, the true number of over-all transfer units. Other parameters needed for this calculation are the Péclet numbers for both phases and the extraction factor, Λ. Results of this model will be described next, as applied to the general case in which the mass-transfer resistance is significant in both phases.

The number of over-all dispersion units, N_{oxD}, was defined by

$$\frac{1}{N_{oxP}} = \frac{1}{N_{ox}} + \frac{1}{N_{oxD}} . \tag{17}$$

A simplified regrouping of the independent variables was shown empirically to be feasible. This regrouping involves defining

$$(PB)_y = \left[\frac{\Lambda}{f_x P_x B} + \frac{1}{f_y P_y B}\right]^{-1} , \tag{18}$$

and the number of over-all dispersion units may be approximated numerically by

$$N_{oxD} = \frac{\ln \Lambda}{\Lambda - 1} \phi + (PB)_y , \tag{19}$$

where

$$f_x = \frac{N_{ox} + 6.8\Lambda^{-0.5}}{N_{ox} + 6.8\Lambda^{-1.5}} , \tag{20}$$

$$f_y = \frac{N_{ox} + 6.8\Lambda^{-0.5}}{N_{ox} + 6.8\Lambda^{+0.5}} , \tag{21}$$

and, tentatively,

$$\phi = 1 - \frac{0.050}{\Lambda(PB)_y^{0.5}(N_{ox})^{0.25}} \tag{22}$$

Correlation is limited to the region where ϕ is positive. Note that in Eq. (19),

$$N_{oxD} \rightarrow \phi + (PB)_y \quad \text{as } \Lambda \rightarrow 1. \tag{23}$$

Solution of these equations for N_{ox} from N_{oxP} involves trail-and-error procedures. One assumes a value for N_{ox} and then computes N_{ox} from Eq. (17) after evaluating N_{oxD} from Eqs. (18) through (22), until agreement is reached. Important assumptions in this treatment are that the packing Péclet numbers and extraction factor remain constant along the length of the extractor.

The calculation method given was derived for liquid-liquid extraction. In extending it to absorption the "X" phase may be either liquid or gas.

For the special case in which $\Lambda = 0$, another technique is applied. This condition exists in gas-absorption columns for cases of vaporization of a pure solvent or absorption followed by a rapid irreversible reaction, and this condition is also approached for extremely soluble and extremely insoluble gases for which the mass-transfer resistance may be assumed to lie essentially within one phase.

Then it develops that[6]

$$N_{oxP} = \ln \left[\frac{N_{ox}(e^{-\lambda_2} - e^{-\lambda_1}) + \lambda_1 e^{-\lambda_2} - \lambda_2 e^{-\lambda_1}}{P_x B (1+4r)^{1/2}} \right], \tag{24}$$

where

$$\lambda_1 = \frac{P_x B}{2} [1 + (1+4r)^{1/2}], \tag{25}$$

$$\lambda_2 = \frac{P_x B}{2} [1 - (1_4r)^{1/2}], \tag{26}$$

and

$$r = \frac{N_{ox}}{P_x B}. \tag{27}$$

This relationship is illustrated graphically in Fig. 23, where N_{oxP} is plotted against N_{ox} for several values of $P_x B$. A simple empirical relation, equivalent to Eq. (24) but explicit in N_{ox}, has been developed by Moon.[8]

$$N_{ox} - N_{oxP} = \frac{0.96(N_{oxp})^2}{P_x B + 0.63}. \tag{28}$$

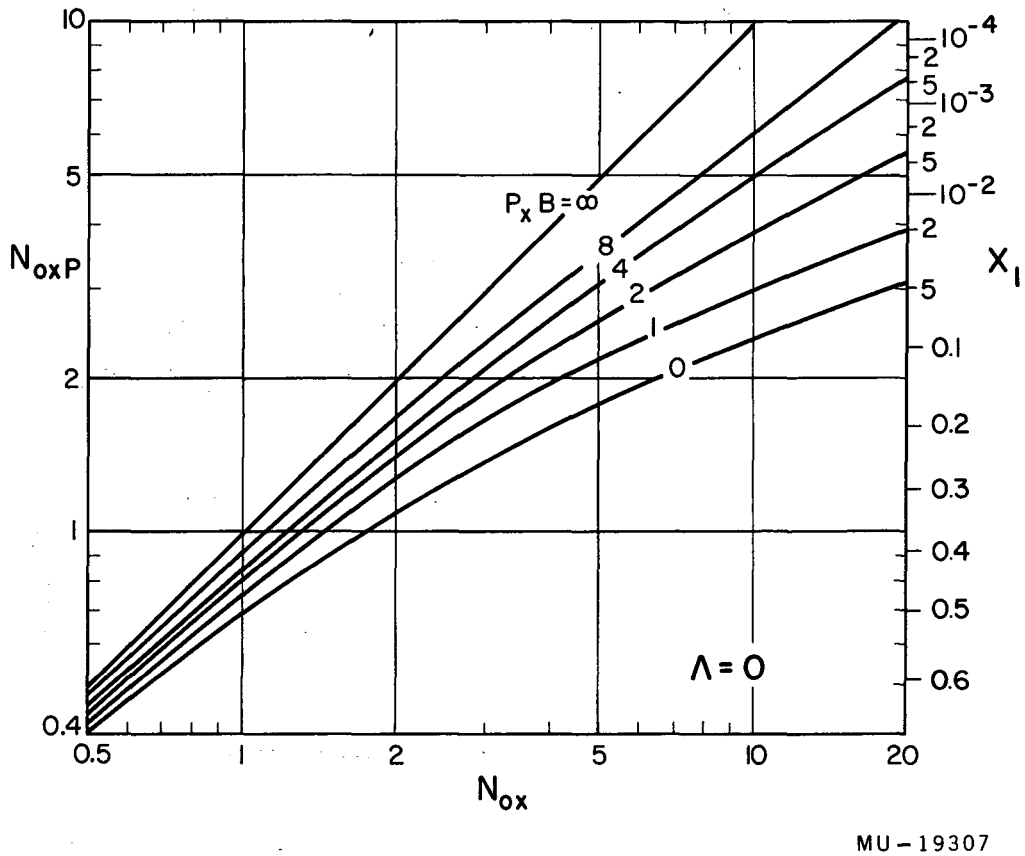

Fig. 23. N_{oxP} as a function of N_{ox} and $P_x B$ with $\Lambda = 0$.

The data of Fellinger[3] for ammonia absorption from air to water were examined to see whether longitudinal mixing contributed a significant effect. Packing Péclet numbers for Fellinger's system were estimated from the correlations of the preceding section. Hence, it was assumed that longitudinal mixing takes place independently of any mass-transfer operation. The conditions of some of Fellinger's runs are given in Table II, along with the results of the practical calculation method.

Table II. Mixing correction for data of Fellinger. Ammonia absorption in a column packed to a depth of 25.5 in. of 1-in. Raschig rings ($L = 4500$ lb/hr-ft^2, x = air phase, and y = water phase).

G (lb/hr-ft^2)	Λ	P_xB	P_yB	N_{oxP}	N_{ox}	H_{oxP} (ft)	H_{ox} (ft)
385	0.0984	23.6	4.30	3.51	4.82	0.605	0.441
600	0.153	19.8	4.30	3.28	4.76	0.646	0.446
800	0.204	16.4	4.30	3.92	7.25	0.542	0.293

The apparent over-all HTU, H_{oxP}, and the true HTU, H_{ox}, are shown as a function of flow rate in Fig. 24. There is an appreciable difference between these values, indicating that mixing had a significant effect on column operation for this case. The factor that contributed most heavily in this particular calculation was the small liquid-phase Péclet number.

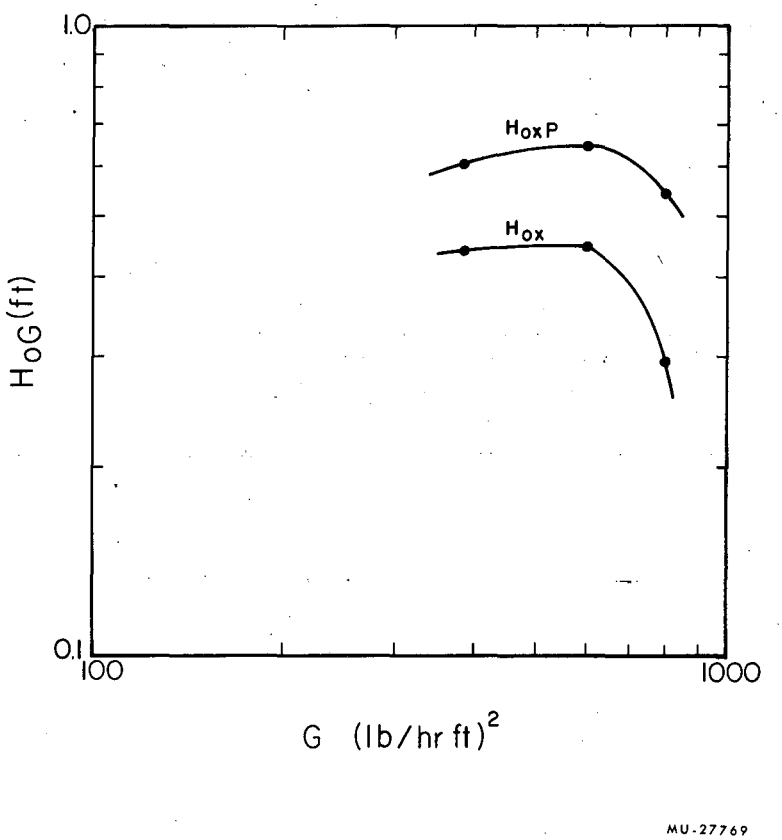

Fig. 24. Mixing correction for data of Fellinger.

We also examined the data of Sherwood and Holloway;[10] they illustrate the application of the mixing correction to a system in which mass-transfer resistance may be assumed to lie entirely within one phase. These investigators have reported HTU values for desorption of oxygen from water by using various standard packings. In this instance the liquid phase is controlling, as evidenced by the extreme insolubility of oxygen in water. Essential data from one set of runs are tabulated below, with the results of the mixing correction indicated by Eq. (28).

Table III. Mixing correction for data of Sherwood and Holloway. Oxygen desorption from water in a column packed to a depth of 6.1 in. with 2-in. Raschig rings ($G=230$ lb/hr-ft^2, and x= water phase).

L (lb/hr-ft)^2	P_xB	N_{oxP}	N_{ox}	H_{oxP} (ft)	H_{ox} (ft)
2000	0.519	0.627	0.956	0.810	0.531
4000	0.651	0.529	0.739	0.960	0.688
12,200	1.66	0.339	0.387	1.50	1.31

A graphical representation is given in Fig. 25, where H_{oxP} and H_{ox} are plotted against the liquid flow rate on a log-log scale. Liquid-phase Péclet numbers were computed by the correlation of Eq. (16) developed in the preceding section.

Again, as in the preceding example, there is an appreciable difference between the apparent and true HTU. In general, one would expect the mixing correction applied to HTU data to be more pronounced for liquid-phase-controlled diffusion than for gas-phase-controlled diffusion, owing to the higher degree of mixing in the liquid phase.

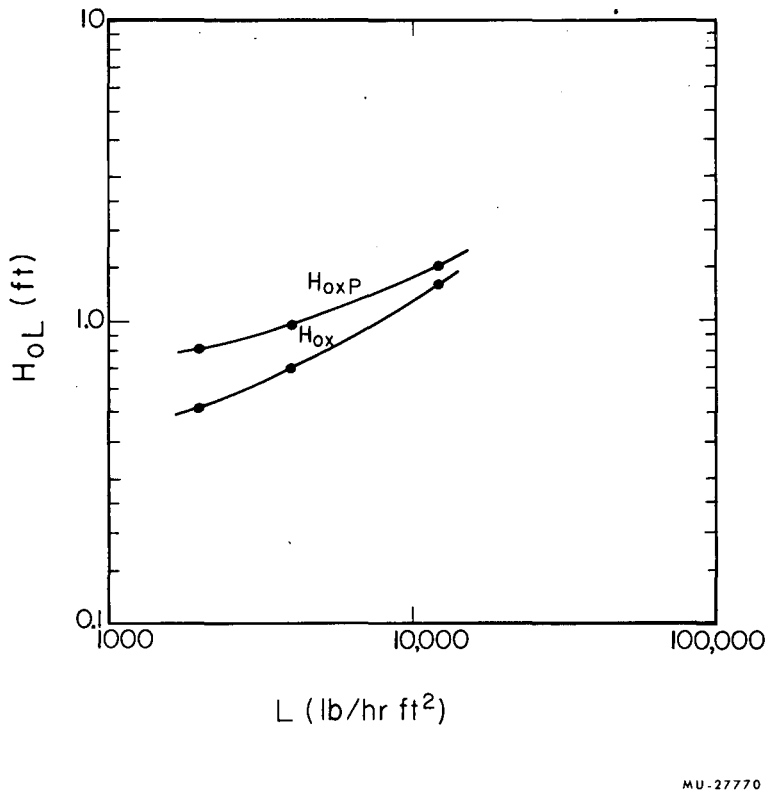

Fig. 25. Mixing correction for data of Sherwood and Holloway.

ACKNOWLEDGMENT

This work was done under the auspices of the U. S. Atomic Energy Commission.

NOTATION

a_p	Packing surface area per unit volume (ft^2/ft^3)
B	h/d_p
C_i	Dimensionless concentration in ith phase
C_0	Magnitude of step concentration-change
d_p	Equivalent-sphere diameter of packing (in.)
f_x, f_y	Weighting factors defined by Eqs. (20) and (21)
E_i	Eddy-dispersion coefficient of ith phase (cm^2/sec)
F	Tangent-angle correction for gas breakthrough curves
F_i	Molar flow rate of ith phase
G	Gas-flow rate ($lb/hr\text{-}ft^2$)
h	Column height
H_{ox}	True over-all height of a transfer unit (ft)
H_{oxP}	Apparent over-all height of a transfer unit (ft)
I_0	Bessel function of zero order, with imaginary argument
l	Mean free path
L	Liquid flow rate ($lb/hr\text{-}ft^2$)
m	Slope of equilibrium curve (mol fraction basis)
N	Column Péclet number
N_{ox}	True number of transfer units
N_{oxD}	Number of over-all dispersion units
N_{oxP}	Apparent piston-flow number of transfer units
P_i	Packing Péclet number of ith phase ($N \times \frac{d_p}{h}$)
$(PB)_y$	Over-all Péclet number defined by Eq. (18)
q_i	Volumetric flow rate of ith phase (ft^3/sec)
r	$N_{ox}/P_x B$
s	Dimensionless midpoint slope of breakthrough curve
t	Time
$(t_r)_i$	Average residence time of ith phase (sec)
T	Dimensionless time

u_i	Characteristic velocity of ith phase
V_i	Column holdup of ith phase (ft^3)
x	Dimensionless concentration (C/C_0)
Y	Midpoint ordinate of gas breakthrough curve relative to the centerline of the chart paper
Z	Dimensionless length of column along direction of flow of the ith phase

Greek Letters

ϵ	Void fraction
λ_1, λ_2	Defined by Eq. (25) and (26)
Λ	Extraction factor (mF_x/F_y)
ψ	Tangent angle of breakthrough curve at midpoint (deg)
μ_n	Defined by Eq. (10)
ϕ	Defined by Eq. (22)

APPENDIX

Sample Calculation for Gas Breakthrough Curve:Run 83 (see Fig. 26).

We use 1-in. Raschig rings,

$L = 5000$ lb/hr-ft^2,
$G = 300$ lb/hr-ft^2,
$C_0 = 6.0$ chart units,
apparent $t_{(x=0.5)}$ corrected for sampler dead time $=19.1-4.5=14.6$ chart units,
and apparent tangent angle at midpoint $= 40.5^\circ = \psi$.

A small correction is applied to the angle because the ordinate is not rectilinear, rather it is curved with a radius equal to the recorder-pen radius.

The correction factor, F, is

$$\frac{\pi/2}{\pi/2 + \sin^{-1}(Y/a)},$$

where

Y = ordinate value where angle is measured relative to the centerline of the chart paper,

and

a = radius of pen, 7.7 cm or 15.4 chart units.

For this case

$Y = +0.4$, therefore, $F = 0.984$.

Then we have

$$s = \frac{dc}{dt} \times \frac{t(x=0.5)}{C_0} = \tan(F\psi) \times \frac{t(x=0.5)}{C_0} = 0.833 \times \frac{14.6}{6.0} = 2.02,$$

$$N = 4\pi s^2 - 0.80 = 51,$$

and

$$P = N \times \frac{d_p}{h} = 51 \times \frac{0.376}{60} = 0.32.$$

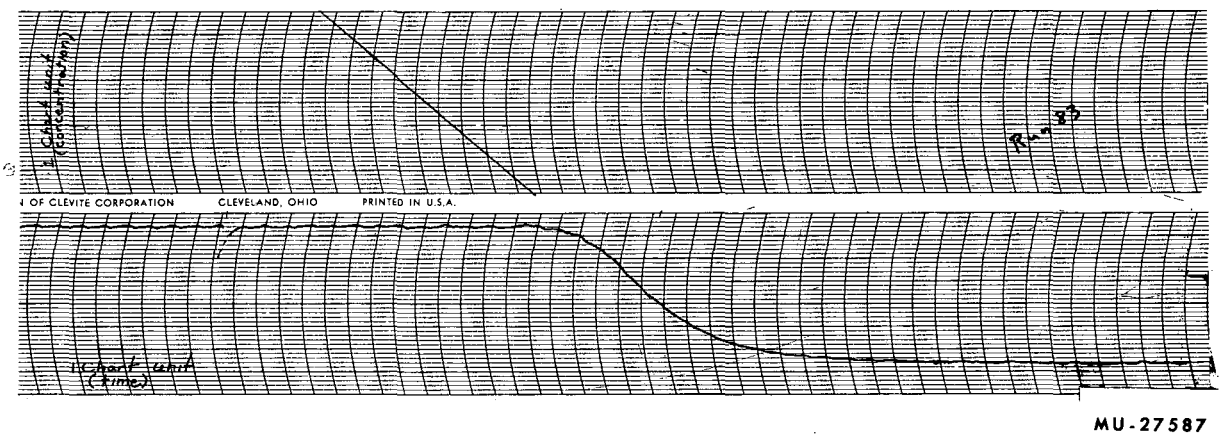

Fig. 26. Typical gas trace-Run 83.

Sample Calculation for Liquid Breakthrough Curve: Run 84 (see Fig. 27).

We use 1-in. Raschig rings,

$$L = 500 \text{ lb/hr-ft}^2,$$

and

$$G = 300 \text{ lb/hr-ft}^2.$$

A. Red Pen

In the run marked Red Pen on Fig. 27 we use:

$$C_0 = 82 \text{ chart units},$$

and

$$\text{apparent } t_{(x-0.5)} = 17.5 \text{ chart units};$$

Sampler dead-time correction:

$$\text{sampler cross section} = \frac{\pi(1.5 \text{ in.})^2}{4(144 \text{ in.}^2/\text{ft}^2} = 0.0123 \text{ ft}^2,$$

$$\text{sampler flow rate} = \frac{5000 \text{ lb/hr-ft}^2 (0.0123 \text{ ft}^2) 16.4 \text{ cm}^3/\text{in.}^3 (1728 \text{ in.}^2/\text{ft}^3)}{3600 \text{ sec/hr } (62.4 \text{ lb/ft}^3)}$$

$$= 7.75 \text{ cm}^3/\text{sec},$$

$$\text{sampler volume above conductivity pins} = 3 \text{ cm}^3,$$

and

$$\text{sampler deadtime} = \frac{3 \text{ cm}^3}{7.75 \text{cm}^3/\text{sec}} = 0.4 \text{ sec} = 0.8 \text{ chart units};$$

$$\text{true } t_{(x-0.5)} = 17.5 - 0.8 = 16.7 \text{ chart units},$$

$$\text{tangent angle at midpoint} = 74 \text{ deg} = \psi,$$

and

$$s = \frac{dc}{dt} \times \frac{t_{(x=0.5)}}{C_0} = \tan\psi \times \frac{t_{(x=0.5)}}{C_0} = 3.49 \times \frac{16.7}{82} = 0.710.$$

From Fig. 4, we get

$$N = 4.6,$$

and then

$$P = N \times \frac{d_p}{h} = 4.6 \times \frac{0.376}{30} = 0.0576$$

B. Black Pen

In the run marked Black Pen on Fig. 27 we use

C_0 = 61 chart units,
apparent t(x=0.5) = 36.5 chart units,
true t(x=0.5) = 36.5 - 0.8 = 35.7 chart units,
tangent angle at midpoint = 58 deg, $\tan\psi = 1.60$,

and

$$s = 1.60 \times \frac{35.7}{61} = 0.938.$$

From Fig. 4, we get

$$N = 9.5,$$

and then

$$P = 9.5 \times \frac{0.376}{60} = 0.0595$$

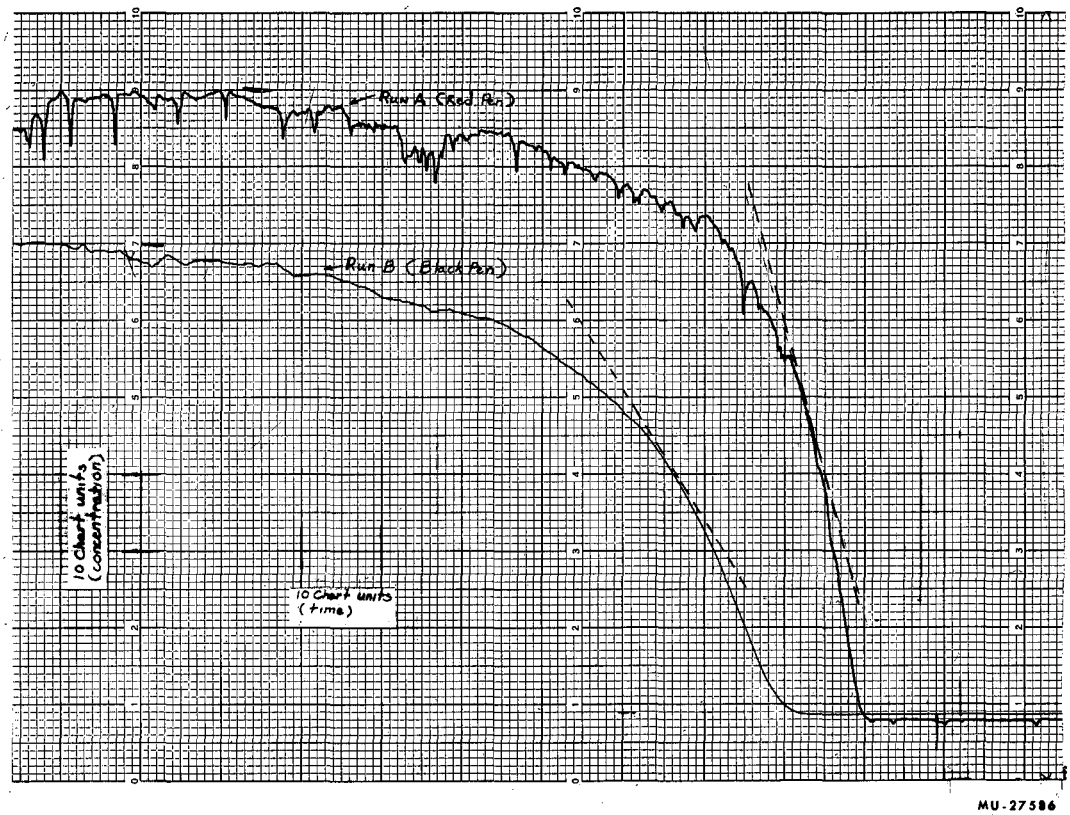

Fig. 27. Typical liquid traces-Run 84.

Estimation of Eddy Diffusivity

Liquid Diffusivity:

Let the subscript x denote the liquid phase; then eddy diffusivity is related to Péclet number by

$$P_x = \frac{d_p U_x}{E_x},$$

where E_x is the eddy-diffusion coefficient and U_x the characteristic velocity. The characteristic velocity $U_x = h/(t_r)_x$, where $(t_r)_x$ is the average residence time of the x-phase. Residence time is related to phase holdup and bulk flow rate by

$$(t_r)_x = \frac{V_x}{q_x},$$

where V_x is the volume holdup of the x-phase in the packing and q_x the bulk volumetric flow rate of the x phase.

Consider the conditions of run 84 where $L = 5000$ lb/hr-ft^2 and $G = 300$ lb/hr-ft.^{2}

Data:

From Eq. (15), $P_x = 0.0581$,

$h = 60$ in. $= 152$ cm,

$d_p = 0.376$ in. $= 0.955$ cm,

$V_x = 0.982$ ft^3(measured),

and

$q_x = 5000$ lb/hr-ft$^2 = 0.0700$ ft^3/sec;

therefore

$$(t_r)_x = \frac{0.982 \text{ ft}^3}{0.0700 \text{ ft}^3/\text{sec}} = 14.0 \text{ sec},$$

and

$$E_x = \frac{dp_h}{P_x(t_r)_x} = \frac{0.955 \text{ cm}(152 \text{ cm})}{0.0581\,(14.0 \text{ sec})} = 178 \text{ cm}^2/\text{sec}.$$

The molecular diffusivity for sodium nitrate diffusion into water is on the order of 10^{-5} cm^2/sec.

Gas Diffusivity

Again consider the conditions of $L = 5000$ lb/hr-ft^2 and $G = 300$ lb/hr-ft^2 (run 83 for gas phase), and let the subscript y denote the gas phase.

Data:

From Eq. (12), $P_y = 0.436$,

$h = 60$ in. $= 152$ cm,

$d_p = 0.376$ in. $= 0.955$ cm,

V_y = total volume X void fraction - $V_x = 9.75$ ft^3,

and

$q_y = 300$ lb/hr-ft$^2 = 3.47$ ft^3/sec;

therefore

$$(t_r)_y = \frac{9.27 \text{ ft}^3}{3.47 \text{ ft}^3/\text{sec}} = 2.67 \text{ sec},$$

and

$$E_y = \frac{d_p}{P_y(t_r)_y} = \frac{0.955 \text{ cm}(152\text{cm})}{0.436\,(2.67 \text{ sec})} = \underline{125 \text{ cm}^2/\text{sec}}.$$

The molecular diffusivity for helium into air as estimated by the equation of Hirschfelder, et al.,[12] is 0.687 cm^2/sec.

REFERENCES

1. A. P. Colburn, Trans. A.I. Ch. E. 29, 174 (1939).
2. A. P. Colburn, Ind. Eng. Chem. 33, 459 (1941).
3. L. Fellinger, Absorption of Ammonia by Water and Acid in Various Standard Packings (Sc. D. Thesis), Massachusetts Institute of Technology, 1941 (unpublished).
4. A. Hennico, (University of California, Berkeley, California), private communication.
5. G. L. Jacques, J. E. Cotter, and T. Vermeulen, Longitudinal Dispersion in Packed Extraction Columns, Lawrence Radiation Laboratory Report UCRL-8658, April 1959 (unpublished).
6. T. Miyauchi, Longitudinal Dispersion in Solvent Extraction Columns: Mathematical Theory, University of California Radiation Laboratory Report UCRL-3911, August 1957 (unpublished).
7. T. Miyauchi, A. McMullen, and T. Vermeulen, Longitudinal Dispersion in Two-Phase Continuous-Flow Operations: Calculation Methods, Lawrence Radiation Laboratory Report UCRL-3911 Rev., March 1960 (unpublished).
8. J. Moon, (University of California, Berkeley, California) private communication.
9. T. Otake and E. Kunugita, Chem. Eng. (Japan) 22, 144 (1958) (in Japanese).
10. T. Sherwood and F. Holloway, Trans. A.I. Ch. E. 36, 49 (1940).
11. A. Stemerding, in Proceedings of the Second European Symposium on Chemical Reaction Engineering, Chem. Eng. Sci. 14, 209 (January 1961).
12. R. E. Treybal, Mass-Transfer Operation (McGraw-Hill Company, Inc., New York, 1955).
13. Tracy T. Word, Longitudinal Dispersion in Packed Gas-Absorption Columns, Lawrence Radiation Laboratory Report UCRL-9844, September 1961 (unpublished).

This report was prepared as an account of Government sponsored work. Neither the United States, nor the Commission, nor any person acting on behalf of the Commission:

A. Makes any warranty or representation, expressed or implied, with respect to the accuracy, completeness, or usefulness of the information contained in this report, or that the use of any information, apparatus, method, or process disclosed in this report may not infringe privately owned rights; or

B. Assumes any liabilities with respect to the use of, or for damages resulting from the use of any information, apparatus, method, or process disclosed in this report.

As used in the above, "person acting on behalf of the Commission" includes any employee or contractor of the Commission, or employee of such contractor, to the extent that such employee or contractor of the Commission, or employee of such contractor prepares, disseminates, or provides access to, any information pursuant to his employment or contract with the Commission, or his employment with such contractor.